Journal of Hydrology 572 (2019) 851–868

Contents lists available at ScienceDirect

Journal of Hydrology

journal homepage: www.elsevier.com/locate/jhydrol

Research papers

Examining the pluvial to nival river regime spectrum using nonlinear methods: Minimum delay embedding dimension

N.O. Aksamit*, P.H. Whitfield

Centre for Hydrology, University of Saskatchewan, Saskatoon, SK, Canada

ARTICLE INFO

This manuscript was handled by A. Bardossy, Editor-in-Chief, with the assistance of Shreedhar Maskey, Associate Editor

Keywords:
Streamflow
Climate change
Pluvial-nival spectrum
Delay embedding space
Nonlinear analysis
False nearest neighbor

ABSTRACT

The nonlinear dynamics of streamflow time series from 667 reference hydrometric stations in North America spanning the pluvial-nival hydrological continuum are explored using minimum embedding dimensions as determined by False Nearest Neighbor (FNN) methods. Simulations using synthetic time series demonstrate that snowmelt dominated time series have lower embedding dimensions than those that are rainfall dominated, and that mixtures of the two processes result in a nearly linear change in the embedding dimension. The majority of the reference hydrometric stations drop below a 1% threshold at a dimension less than 30, showing a high degree of natural complexity in the signals ranging from annual snowmelt to weather-driven pseudo-stochastic systems. A less restrictive threshold, 5% is suggested to be more appropriate for streamflow time series. Time series smoothing impacts the embedding dimension and over-smoothing results in incorrect reductions of embedding dimensions. The relationship of the embedding dimensions to watershed and statistical properties of streamflow record showed the lowest embedding dimensions are restricted to large drainage areas, high elevations, and large mean annual flows and variance, high autocorrelations, and large fractions of the records with only small changes in magnitude. Times series that have a large proportion of consecutive days of equal streamflow typically result in higher embedding dimensions. Mapping of the embedding dimension shows spatial patterns related to the streamflow generating processes and geographical features. The use of embedding dimension resolved different dynamics across the hydrological continuum for rainfall to snowmelt over many climate zones. Changes in the embedding dimension might indicate process changes related to climate variability and change.

1. Introduction

Rainfall-driven and snowmelt-driven hydrological systems exhibit distinct streamflow behavior and shape their landscapes differently. In changing climates, the necessity of a better understanding of the distinguishing factors of pluvial and nival rivers has increased (Burn and Whitfield, 2017). For example, if typically nival rivers receive more rain events in the future, flood generating mechanisms will change, as will the magnitude and frequency of rain-on-snow floods. The ability to diagnose such process changes in hydrology is still limited. The present research seeks to illuminate and quantify the pluvial to nival spectrum through nonlinear time series analysis of streamflow time series from a large collection of North American reference hydrological stations. The ability to quantify the position on this spectrum based upon historical data can contribute to detecting changes in process related to future climate variations and change.

Hydrology is fundamentally a study of nonlinear processes conducted extensively with linear methods (Amorocho, 1963, 1967). Schertzer et al. (2010) argue that simplistic approximations in linear operational hydrological models are divorced from hydrological theory. This need not be the case as the real-world dynamics of hydrological systems that appear to be highly variable, complex, and often random may be diagnosed, reconstructed, characterized, and modelled using mathematically rigorous procedures (Coulibaly and Baldwin, 2005; Huffaker et al., 2017). Operational hydrology often ignores nonlinear aspects included in theoretical hydrology (Schertzer et al., 2010).

Seasonal patterns of streamflow and other hydroclimatic variables is a widely covered topic in hydrology. Flow regime classification, the classification of hydrographs based upon streamflow generating mechanisms, or other common hydrological features, seldom has included nonlinear techniques because of the difficulty of the methods (Dooge, 1986). Objective methods have been attempted with shape and magnitude classification for proglacial stream hydrographs (Hannah et al., 2000), or classifications of patterns of peaks, and their timing, to

* Corresponding author at: Institute for Mechanical Systems, Swiss Federal Institute of Technology (ETH), Zurich, Switzerland.
E-mail address: naksamit@ethz.ch (N.O. Aksamit).

https://doi.org/10.1016/j.jhydrol.2019.03.058
Received 26 October 2018; Received in revised form 13 March 2019; Accepted 14 March 2019
Available online 16 March 2019
0022-1694/

associate sites. The latter methods suffer at larger scales and in complex terrain, where differences in latitude and elevation result in the same pattern being identified in separate clusters (Fleming et al., 2007). Swain et al. (2016) used nonlinear techniques (self-organized maps and kernel principle components analysis) to classify streamflow signatures, and found nonlinear methods outperformed linear approaches (Principal Components Analysis and k-means). Furthermore, Sivakumar et al. (2007) make the point that linear tools such as autocorrelation and power spectrum may not be adequate for studying system complexity; where the use of nonlinear concepts is necessary.

It is well known that climatic variables and trends influence hydrological regimes and complicate classifications. Fleming et al. (2007) showed that ocean circulation patterns such as ENSO and the Pacific Decadal Oscillation have different impacts on different streamflow regimes, or rather the streamflow generating processes. Hannaford and Buys (2012) examined trends in flow regimes in the UK in relation to climate and observed increased winter flows and high flows associated with increased rainfall and spatial heterogeneity in trends. Arnell and Gosling (2013) examined how indicators of hydrologic regime might be affected in a future climate where shifts in timing of snowmelt is an indicator. Coopersmith et al. (2014) demonstrated regional differences in runoff regime in the United States measuring shifts in indicators of regimes and that the expansion of the regimes from the American southeast to the north and west generally reflect the projected increased role of precipitation and decrease in snow. Untangling how changes in the climatic system affect hydrological processes is a complex nonlinear problem.

Nonlinear time series analysis is a rich field of mathematics involving many methods adapted from the study of dynamical systems (Kantz and Schreiber, 2003). A time series can be viewed as a one-dimensional measurement of a dynamical system, and the behavior and evolution of the full system can be represented and analyzed in a phase space. Phase Space (or state space) is an abstract construction that allows a dynamical system to be presented in multiple dimensions, each coordinate representing a key feature of the system, and each point representing a specific “state.” If one considers all the hydrological processes that exist in a watershed as components of a dynamical system, a few processes may dominate and result in a low dimensional system. As more processes exist, or the more complex the processes (and their timing), the higher the dimension of the dynamical system becomes.

The time evolution of a hydrological system can be represented in phase space, but, as in all natural sciences, hydrologists are only able to obtain measurements of a subset of the active hydrological process. This means hydrologists always work with a lower dimensional phase space that represents the state of a watershed through a finite number of hydrological variables (e.g. streamflow, meteorology, ground water) that are measured at discrete times. Thus, attempting a full phase space representation is classically problematic as all the relevant variables are not always measured. Takens’ theorem (Takens, 1981), fortunately, proves that the full behavior of a dynamical system can be studied by looking at a time delay embedding of a subspace of the full phase space. For hydrologists, the implication of Takens’ theorem is that the dimension of the dominant dynamics in a basin can be identified from just the streamflow time series. Furthermore, if a dynamical system contains a strange attractor of dimension m, Takens’ theorem and the Whitney embedding theorem prove that this attractor can be fully unfolded in an embedding space of dimension $2m + 1$. This minimum embedding dimension can be considered a metric of complexity or stochasticity of the processes in the basin (Sivakumar and Singh, 2012).

From a hydrological perspective, a time-delay embedded time series may be low-dimensional if there is consistent magnitude and timing of a dominant runoff process. Through the choice of the delay parameter τ, this process may be attributed to short or long “cycles” and trends in precipitation. A high embedding dimension may be caused by variable timing of runoff (such that the delay τ is insufficient to return the embedded time series to the same neighborhoods of the phase space), variable magnitude, the presence of stochastic processes, or other complex mechanisms.

Kennel et al. (1992) explored how to determine the acceptable minimum embedding dimension by examining nearest neighbors. The embedding dimension allows a time-delay reconstruction of a phase space that then illustrates the system dynamics (Kostelich and Yorke, 1990). For physicists, the recommended procedure seeks to reduce the number of false nearest neighbors to less than 1% (Kennel et al., 1992, 1997) though 5% may be sufficient for hydrologists! Kennel et al. (1992) proposed the geometric unfolding method to determine the number of false nearest neighbors that was used here. This technique has seen limited application in hydrology and can be supplemented with recurrence plots to visualize recurrent patterns in a time series, such as by Zbilut and Webber (1992) and March et al. (2005). Khatibi et al. (2012) investigated chaotic behavior in river stage and discharge time series using five nonlinear methods: phase-space reconstruction, false nearest neighbors, correlation dimension, Lyapunov exponents, and a local approximation method. They showed that low-dimensional chaotic structure exists in the two time series studied.

Mann et al. (1995), Lall and Mann (1995), and Lall et al. (1996) demonstrated early connections between decadal climate variation and the variations in the volume of Great Salt Lake, a 100,000 km^2 closed basin, suggesting that decadal variations in volume follow low-frequency shifting of storm tracks. Abarbanel et al. (1996) and Abarbanel and Lall (1996) examined this reconstructed 1842–1992 15-day time series of lake volume (Sangoyomi et al., 1996) using nonlinear methods including FNN and showed that the system dynamic has an embedding dimension of 4 with components lagged by 6 months. This large basin smooths a large number of atmospheric and climatological motions reducing the complexity but retaining its long-term climate sensing. While a number of analyses of climate and weather data find low dimensional attractors (e.g. Abarbanel and Lall, 1996; Lall et al., 1996 and others), Lorenz (1991) indicates that the actual climate attractor is likely to be of much higher dimension and gives several reasons for evidence of low-dimensional representations. Abarbanel and Lall (1996) suggest that analyses similar to those they present might work for large rivers (e.g. Mississippi) (where the smoothing of the climate signal is large), but small streams may be more difficult to analyze, either because of increased complexity in the dynamics or because of a relatively poor signal to noise ratio in the data.

Sivakumar et al. (2002) investigated correlation dimension as an indicator of low-dimensional chaotic structure in hydrological time series. Using monthly runoff for 48 years, the correlation dimension was in agreement with the optimal embedding dimension of the phase space, suggesting it could make a reliable indicator. We would comment that using monthly data removed so much noise and structure from the time series as to not be a sufficient test as demonstrated below. Sivakumar (2004) proposed a procedure to identify dominant processes that used correlation dimension to quantify the number of processes, expert knowledge to identify the processes, and a sensitivity analysis to order the processes by dominance. They suggest that more effort be placed on finding patterns and ‘hidden order’.

Sivakumar et al. (2007) explored the classification issue from the perspective of a simple phase-state reconstruction technique; representing a multidimensional system using a single variable time series through a delay coordinate procedure. The complexity of the reconstruction can then be used to classify systems as low, medium or high, depending on a user-chosen metric for whichever embedding dimension was used (Sivakumar et al., 2007). Sivakumar and Singh (2012) argue that hydrological systems are appropriate for such a classification. Applying the correlation dimension method to monthly streamflow time series from more than 100 watersheds they describe four categories: low, medium, and high complexity and unidentifiable (Sivakumar and Singh, 2012); this classification scheme provided some local homogeneity, but exceptions existed. In contrast, Tongal and

Sivakumar (2017) consider a cross-entropy clustering method that used embedding dimension, sample entropy, and a coefficient of variability; the combination of nonlinear and linear variables successfully determined distinct flow generating mechanisms in different parts of Australia.

Vignesh et al. (2015) used a false nearest neighbor (FNN) algorithm to examine the spatial variability over a region of the United States using monthly streamflow data. Vignesh et al. (2015) varied the delay time values (monthly, seasonal, annual, autocorrelation, and the average mutual information) and found that the FNN embedding dimensions may or may not change with different delay times. In contrast to a fixed %FNN threshold, such as by Abarbanel et al. (1993), Vignesh et al. (2015) simply use the embedding dimension of the lowest %FNN. By mapping FNN embedding dimension, Vignesh et al. (2015) demonstrate differences in variability in streamflow dynamics across the US; lower delay times result in wider variability in the embedding dimension in the west than in the east. Vignesh et al. (2015) also compared FNN dimensions to catchment characteristics and streamflow statistical properties. Low embedding dimensions occur in both small and large drainage basins but high embedding dimensions are associated only with small drainage areas. Low embedding dimensions occur at both low and high elevations, but high values are only at low elevations. High embedding dimensions are associated only with low annual mean flows. Since embedding dimension and coefficient of variation are both measures of variability, nonlinear and linear, there has been shown to be a positive relationship between them (Vignesh et al., 2015).

The previous review of the field indicates that using the minimum embedding dimension as an indicator of the hydrologic regime is a novel application of the technique. The basic hypothesis of the present research is that a simple annual snowmelt signal (e.g. a modified sine curve) will reflect a low-dimensional dynamical system and thus will have a low minimum embedding dimension. Respectively, pluvial systems may have strong seasonal patterns but are more stochastic at single day time steps than snowmelt, and cannot be fully unfolded at low dimensions and thus the false nearest neighbor calculations are expected to produce higher minimum embedding dimension. Expanding our focus beyond low-dimensional systems allows a consideration of chaotic or stochastic signals not as merely evidence of meaningless noise, but rather as signals representing a poorly understood, and much more complex weather-driven process (Abarbanel and Lall, 1996). It is shown that excessive smoothing may have the adverse effect of destroying information that is actually characteristic of a hydrologic regime, and it should not be assumed a priori that hydrological systems can represented with only a few state variables.

The present study uses both synthetic time series that mimic snowmelt, rainfall and noise contributions and streamflow time series from 667 hydrological reference sites in North America. This allows the embedding dimension to be explored in some detail to demonstrate that minimum embedding dimensions provide information about separation of these two processes. A sensitivity analysis was also conducted to assess the effects on minimum embedding dimension (D_E) several hydrologically important influences: [1] how long and/or how much of a streamflow record is required to determine D_E, [2] does the scaling of the time series affect D_E, [3] does the basin area and elevation affect D_E, [4] how much averaging is required to reduce random noise to the point where a D_E estimate can be found, and what happens if oversmoothing results, and [5] how is D_E related to statistical properties of the time series. The utility of the method is demonstrated by estimating the minimum embedding dimension for hydrological reference sites in North America and exploring the spatial distribution of D_E.

2. Methods

The theoretical basis for the False nearest neighbor methodology is outlined first, followed by the nature of the streamflow time series from reference hydrologic networks and the synthetic time series used in method testing.

2.1. Delay embedding spaces and false nearest neighbors

For a one-dimensional (time series) measurement of a nonlinear system, $x(t)$, a time-delay reconstruction can be used to view the underlying dynamics. The parameterized curve $\boldsymbol{y_n}(t) = (x(t), x(t+\tau), \cdots, x(t+\tau(n-1)))$, where τ is a choice of time delay and n is the dimension chosen to unfold the dynamics of the system, traces out an orbit in the system. The convention used in the present research is a time delay at which the average mutual information (AMI) is one-fifth of the value attained at no time delay (cf. Abarbanel et al., 1993) and will not be a focus of the current research. The choice of one-fifth AMI instead of the time of first local minimum was necessary as some time series had AMI that was monotonically decreasing.

The central premise of this study is to find an appropriate dimension n at which the full dynamics of the system can be unfolded. While there are several techniques to estimate this value, the geometric approach of Kennel et al. (1992) to identify the minimum dimension through identification of False Nearest Neighbors (FNN) is widely used and sufficient for comparison of hydrological systems. An efficient FNN computation script written in MATLAB from the University of Potsdam (http://tocsy.pik-potsdam.de/CRPtoolbox/) (Marwan et al., 2007) was used. This code calculates the embedding dimension of the total time series with a cost-saving computation based on identifying FNN for many subsections of the time series and can result in small variability from one approximation to the next. As the focus on this research will not be on identifying behavior that results in each dimension, this small variability was deemed acceptable and did not influence the results.

Detailed explanations of the theory of FNN can be found elsewhere (e.g. Abarbanel et al., 1993; Kantz and Schreiber, 2003), but a brief explanation is given here for completeness. For a given time t, and a point $\boldsymbol{y_n}(t) = (x(t), x(t+\tau), \cdots, x(t+\tau(n-1)))$in the orbit of our time series in an embedding space of dimension n, the rth nearest neighbor to $\boldsymbol{y_n}(t)$, call it $\boldsymbol{y_n^r}(t)$, is a point at the Euclidean distance

$$R_n^2(t, r) = \sum_{k=0}^{n-1} [x(t+k\tau) - x^r(t+k\tau)]^2$$

Kennel et al. (1992) use two criteria that may designate this neighbor as "false" by comparing $R_n^2(t, r)$ to $R_{n+1}^2(t, r) = \sum_{k=0}^{n} [x(t+k\tau) - x^r(t+k\tau)]^2$, the distance of the same two orbital points in the next higher delay embedding dimension. The first criterion eliminates points that only appear close in a given dimension because the orbit is not fully unfolded. In a higher dimension where the orbit is actually unfolded, the points are relatively far apart. This is demonstrated in Fig. 1 where, for simplicity, our orbit of points all fall on a circle. Points 'A' and 'B' on the circle appear close when projected onto one dimension ($n = 1$), but in reality are far apart when the orbit is fully unfolded ($n = 2$). Points 'A' and 'C' are examples of true nearest neighbors. This criterion is formally stated as $\boldsymbol{y_n^r}(t)$ is a FNN to $\boldsymbol{y_n}(t)$ if

$$\left[\frac{R_{n+1}^2(t, r) - R_n^2(t, r)}{R_n^2(t, r)}\right]^{1/2} = \frac{|x(t+n\tau) - x^r(t+n\tau)|}{R_n(t, r)} > R_{tol}$$

where $R_{tol} \geq 10$ is sufficient.

The second criterion helps manage the influence of high-dimensional noise in nonlinear systems that have a limited time series length. If the closest point to $\boldsymbol{y_n}(t)$ is actually not close, that is $R_n(t, r)$ is of the order of the width of the orbit, and $R_{n+1}(t, r)$ is also large, then $\boldsymbol{y_n^r}(t)$ should also be considered false. Formally

$$\frac{R_{n+1}(t, 1)}{R_A} > A_{tol}$$

where $R_A^2 = \frac{1}{N}\sum_t [x(t) - \bar{x}]^2$ and $\bar{x} = \frac{1}{N}\sum_t x(t)$ and N is the length of

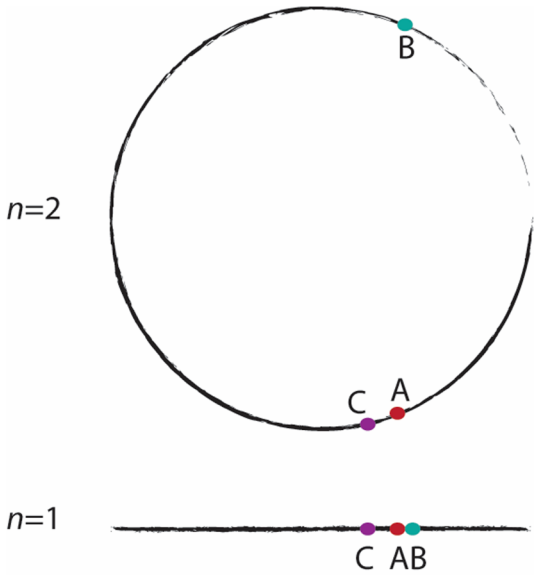

Fig. 1. Illustration of an orbit sparsely covering a circular attractor. Points A and B are false nearest neighbors in dimension $n = 1$, whereas A and C are true nearest neighbors when the orbit is fully unfolded in $n = 2$.

the time series.

In the Kennel method, the first dimension D_E at which the percent of nearest neighbors that are false drops below 1% is then defined as D_E. We found that the 1% threshold was too restrictive for streamflow data that contains significant noise and about 14% of the cases failed to converge (Appendix). Instead, a threshold of 5% resulted in only one case which did not converge, so that threshold was used for the remainder of this study.

It is worth noting that the two criteria are also unaffected by linear translation and rescaling. Consider a time series $x(t)$ and a modified series $y(t) = ax(t) + b$, where a and b are real numbers, and their respective metrics $R_{n,x}$, $R_{n,y}$, $R_{A,x}$, and $R_{A,y}$.

$$R^2_{n,y}(t, r) = \sum_{k=0}^{n-1} [y(t + k\tau) - y^r(t + k\tau)]^2$$

$$= \sum_{k=0}^{n-1} [ax(t + k\tau) + b - ax^r(t + k\tau) - b]^2$$

$$= a^2 \sum_{k=0}^{n-1} [x(t + k\tau) - x^r(t + k\tau)]^2$$

$$= a^2 R^2_{n,x}(t, r)$$

$$\text{Thus, } \left[\frac{R^2_{n+1,y}(t,r) - R^2_{n,y}(t,r)}{R^2_{n,y}(t,r)}\right]^{1/2} = \left[\frac{a^2R^2_{n+1,x}(t,r) - a^2R^2_{n,x}(t,r)}{a^2R^2_{n,x}(t,r)}\right]^{1/2}.$$

$$= \left[\frac{R^2_{n+1,x}(t,r) - R^2_{n,x}(t,r)}{R^2_{n,x}(t,r)}\right]^{1/2}$$

Similarly,

$$\bar{y} = \frac{1}{N}\sum_t ax(t) + b = \frac{1}{N}\left[Nb + a\sum_t x(t)\right] = b + a\bar{x}$$

$$R^2_{A,y} = \frac{1}{N}\sum_t [y(t) - a\bar{x} - b]^2 = \frac{1}{N}\sum_t [ax(t) - a\bar{x}]^2 = a^2R^2_{A,x}$$

and $\frac{R_{n+1,y}(t,1)}{R_{A,y}} = \frac{R_{n+1,x}(t,1)}{R_{A,x}}$. This implies it is not necessary or beneficial to standardize the streamflow prior to analysis. It is not the mean flow or the absolute range of streamflow values measured that determines D_E, but only the dynamics of the flow.

FNN were calculated for embedding dimensions ranging from 1 to 30 for each time series. A transition to a dynamical system with more noise, or with more stochastic determinism, results in more FNN at higher dimensions and generates potentially spurious D_E requirements (Kennel et al., 1992). This measure of complexity may help quantify where a basin exists on the spectrum of pluvial to nival as determined by a river streamflow time series. Additionally, non-stationarity in the hydrographs and year-to-year shifts on the pluvial-nival spectrum will also add complex dynamics to the system and potentially increase D_E.

An example of the FNN embedding dimension estimate applied to the x-component of the classic Lorenz system can be seen in Fig. 2. This particular system is governed by the system of ordinary differential equations

$$\frac{dx}{dt} = 10(y - x),$$

$$\frac{dy}{dt} = x(28 - z) - y,$$

$$\frac{dz}{dt} = xy - \frac{8z}{3},$$

and the strange attractor is fully unfolded in three dimensions (shown in Fig. 2a). The color of the parametric curve varies with rescaled time from $t = 0$ to $t = 1$ as seen in the color bar. The effect of adding random sections of uniformly distributed noise to 30% of the time series $x(t)$, potentially representative of signal noise or an additional complementary stochastic process, is seen in Fig. 2b. Here, the percent of FNN per embedding dimension for the clean signal $x(t)$, and noisy signals $x_{noise}(t)$ are displayed. For the clean signal, the percent of FNN drops below 1% at $n = 4$ (and reaches 0% at $n = 7$) which is sufficient

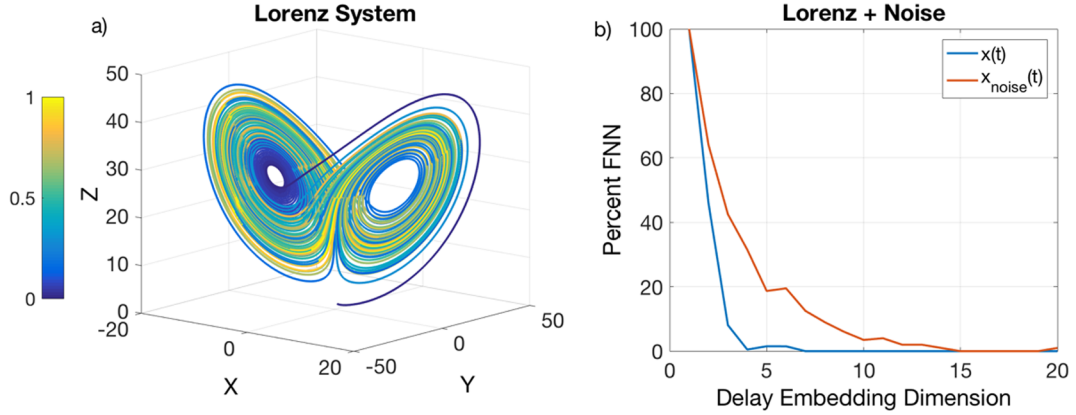

Fig. 2. (a) Phase space plot of the classic Lorenz system with $\sigma = 10$, $\rho = 28$, and $\beta = 8/3$. The parametric curve is colored following time along a rescaled timescale from 0 to 1. Subplot (b) displays the false nearest neighbor calculations for the x-coordinate of the Lorenz system in (a) with and without the addition of random periods of normally distributed noise (2σ(x(t)).

for the Lorenz attractor of dimension $m = 2.06$ according to the Whitney embedding theorem. The amplitude of the added noise was twice the standard deviation of $x(t)$ and increased D_E to 15. It is worth noting, the FNN estimates of D_E were unaffected if the noise was added to the entire time series, as intended by the algorithm design.

2.2. Dataset

The daily streamflow time series used in the following analysis consists of records from 462 USGS reference hydrological stations in the contiguous United States, Hawaii, Alaska, and Puerto Rico as well as 205 reference sites in Canada. Reference hydrological stations were chosen as they are thought to be minimally affected by land use changes and their dynamics only vary with time as a result of climate (Whitfield et al., 2012). The time series of streamflow were required to span at least 40 years, but measurement gaps resulted in a length of data ranging from 27 to 107 years. Prior to FNN calculations, time series of streamflow were smoothed by a 5-day sliding average. This is in accordance with the work of (Whitfield, 1998) that suggests a smoothing of high-frequency components shorter than five days allows a fairer comparison between large and small streams.

A sensitivity analysis was conducted to examine the effect of the amount of smoothing on D_E for all stations in an East to West transect between 38.5°N and 39.5°N and all stations in a North to South transect between 114.5°W and 116.5°W. These bands were chosen as they included a large geographic span of stations and did not result in an overly burdensome number of extra calculations. D_E was calculated for the entire duration of each time series in the transects with sliding-window sizes varying from 2 to 30 days during preprocessing.

Since climate and weather are largely non-stationary and the method here treats streamflow data as stationary, a sensitivity analysis that examined the effect of time series length was also conducted for the same transects of stations. D_E was calculated with a fixed sliding-window size of 5 days with the length of series ranging from 10% to 66% of the entire series length. D_E was calculated for multiple sections of the original time series at each shortened length (10, 4, 4, 2, and 2 sections for 10%, 25%, 33%, 50%, 66% respectively) with the start dates chosen randomly in the series.

Basin drainage area and elevation and streamflow record statistical properties were examined to assess how they may be related to D_E. Statistical properties included mean annual flow, the standard deviation, and the autocorrelation of the streamflow record at a time lag equivalent to that used for the D_E calculation. Some of the streamflow records contain extended periods of zero discharge and we calculated the fraction of the total records where there was no change in flow from one day to the next to address this.

2.3. Synthetic signals

To further test the theory that FNN can help classify hydrographs on a continuum from rainfall to snowmelt driven systems, synthetic 50-year time series of river flow were generated. Three fundamental building-block mechanisms were created to generate synthetic streamflows. These include rainfall, snowmelt and white noise. Linear combinations of the three components were varied and D_E was computed to identify the effect of the transition from a snowmelt to a rainfall driven system. Examples of three different synthetic streamflows can be found in Fig. 3.

The presence of rainfall contribution to streamflow was arbitrarily chosen to occupy no more than 30% of the time series. The start date of the influence of a rainfall event was randomly chosen in the time series as was a random duration of 1–5 days. During these 1-to-5-day periods, the rainfall signal, $rf(t)$, consisted of uniformly distributed noise with values in the open set (0,1). The remaining rainfall signal consisted of zeros. The fundamental snowmelt signal, $sm(t)$, consisted of a rescaled sine curve with a period of 1 year and a range of [0,1]. The sine curve was unchanged for two hundred days of the year surrounding the maximum. The remaining days were set to a fixed base flow equal to the 200th day of the snowmelt oscillation. Constant uniformly distributed random values, $n(t)$, were also added to the time series.

The final synthetic river flow was of the form

$$F(t) = a \cdot rf(t) + b \cdot sm(t) + c \cdot n(t) \quad (1)$$

where $a + b + c = 1$. Values of a ranged from 0 to 0.9 and c was fixed at 0.1. The same preprocessing and FNN calculations described in the previous section were applied to these synthetic time series.

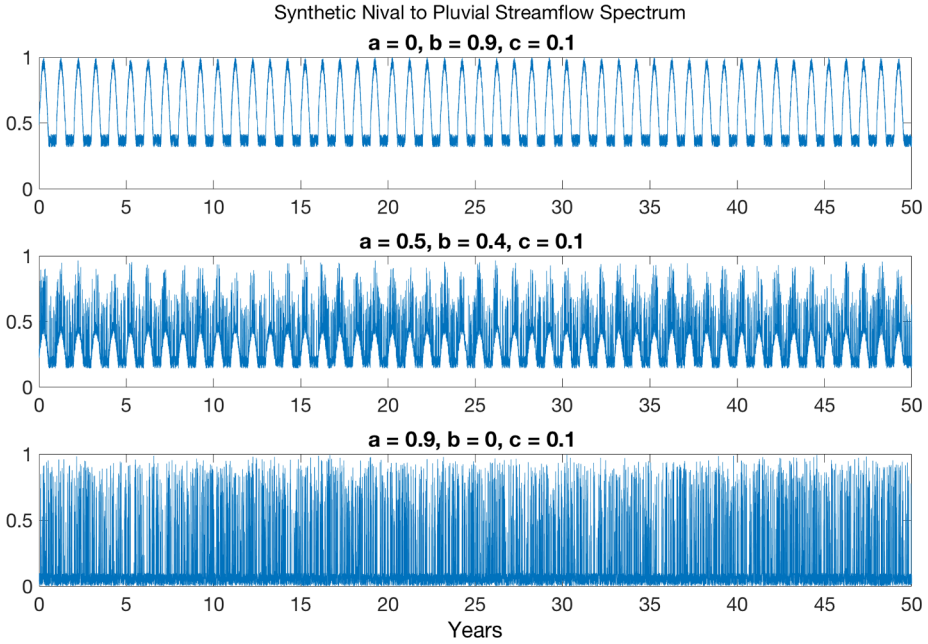

Fig. 3. Synthetic streamflow time series generated from Eq. (1) showing a transition from nival (top) to pluvial (bottom) systems. Coefficients a, b, and c correspond to weights for rainfall, snowmelt, and white noise, in Eq. (1) respectively.

3. Results

3.1. Synthetic data

Synthetic streamflow time series as described in Section 2.3 were generated and analyzed to test whether increasing the relative amplitude of random days of rainfall contribution to streamflow would increase the embedding dimension from a simulated nival baseline. A plot comparing the minimum delay embedding dimension of the synthetic river signals versus the value of coefficient a in Eq. (1) can be found in Fig. 4a. As the rainfall coefficient a in Eq. (1) increased from 0 to 0.9, the minimum delay embedding dimension increased nearly linearly from 5 to 13. In Fig. 4b, the increase of %FNN for each embedding dimension for increasingly pluvial regimes is also displayed. Fig. 4 indicates that D_E and False Nearest Neighbors could be used as a measure of the shift in runoff in a simple nival to a pluvial transition.

As a further investigation in the ability to diagnose changes in the streamflow generating processes, a synthetic time series was generated that spanned 100 years with a linear transition of (a,b) = (0, 0.9) (Nival) at year 1 to (a,b) = (0.9, 0) (Pluvial) at year 100. Minimum embedding dimensions were calculated for consecutive 10 (and 20) year subsections to see if D_E could identify the regime change over time. As could be suspected by the previous synthetic time series analysis, the embedding dimension steadily increased with time from $D_E = 6$ in years 1–10 to $D_E = 12$ in years 91–100. Results using 20-year subsections were similar. This indicates potential for diagnostic applications in climatic regions undergoing transitions from snowmelt to rainfall dominant processes and is further investigated with real streamflow time series in Section 3.2.

It should be noted that the synthetic time series were unable to attain the same level of complexity, and the same range of minimum embedding dimensions, as the natural signals. This is understandable because of their fundamentally simple construction and the ability of the FNN algorithm to disregard white noise (Kennel et al., 1992).

3.2. Hydrological network analysis

The minimum delay embedding dimension was computed for all 667 stream flow time series. Values ranged from 3 to a maximum possible dimension of 30 and can be seen in Fig. 5. The one series where the percent of FNN never dropped below 5% is marked in Fig. 5 as having an embedding dimension of 31, outside the range of calculated values. This time series (Dry Creek at Union City, CA) did eventually drop below 5% FNN at a dimension of 50.

A transition to lower embedding dimensions, suggesting less complexity in the flow, can be seen in much of the colder, snow dominated, Northern regions of Fig. 5, as well as in the major mountain ranges in the east and west. A complementary plot computed at the 1% threshold

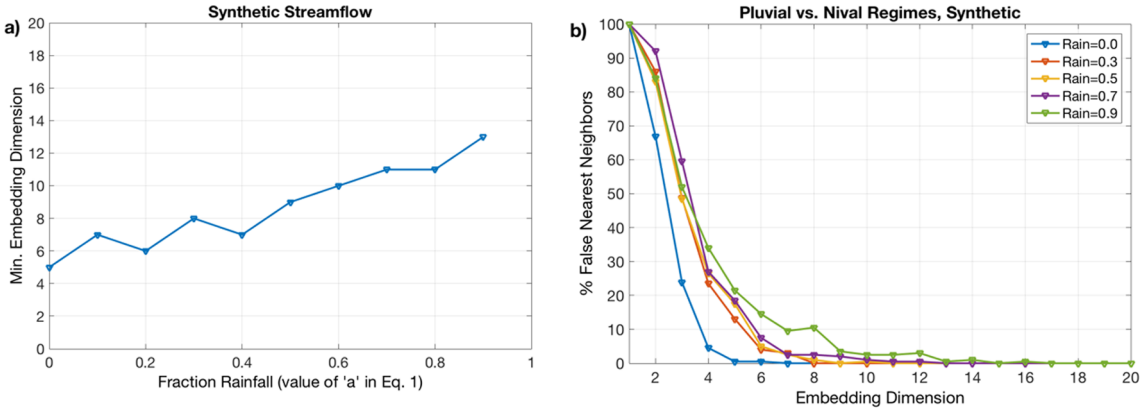

Fig. 4. (a) Minimum delay embedding dimensions for synthetic stream flow as a function of fractional rainfall from Eq. (1), (b) shows the change in % false nearest neighbors as a function of embedding dimension for increasing proportion of rainfall and decreased snowmelt. In all examples the noise component 'c' was 0.1, so rain + snow = 0.9.

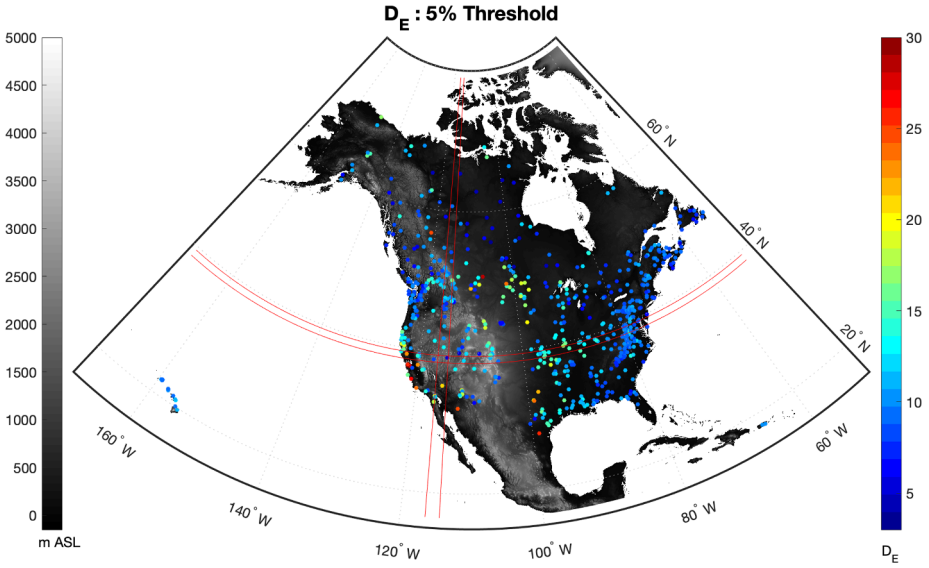

Fig. 5. Minimum delay embedding dimensions for streams across USA, including Hawaii and Puerto Rico, and Canada as calculated with the Kennel et al. (1992) false nearest neighbor algorithm and an FNN threshold of 5%. The red lines indicate a north-south and an east-west transect from which stations were selected for additional investigation and sensitivity analysis and the underlying grayscale map shows topography. (For interpretation of the references to color in this figure legend, the reader is referred to the web version of this article.)

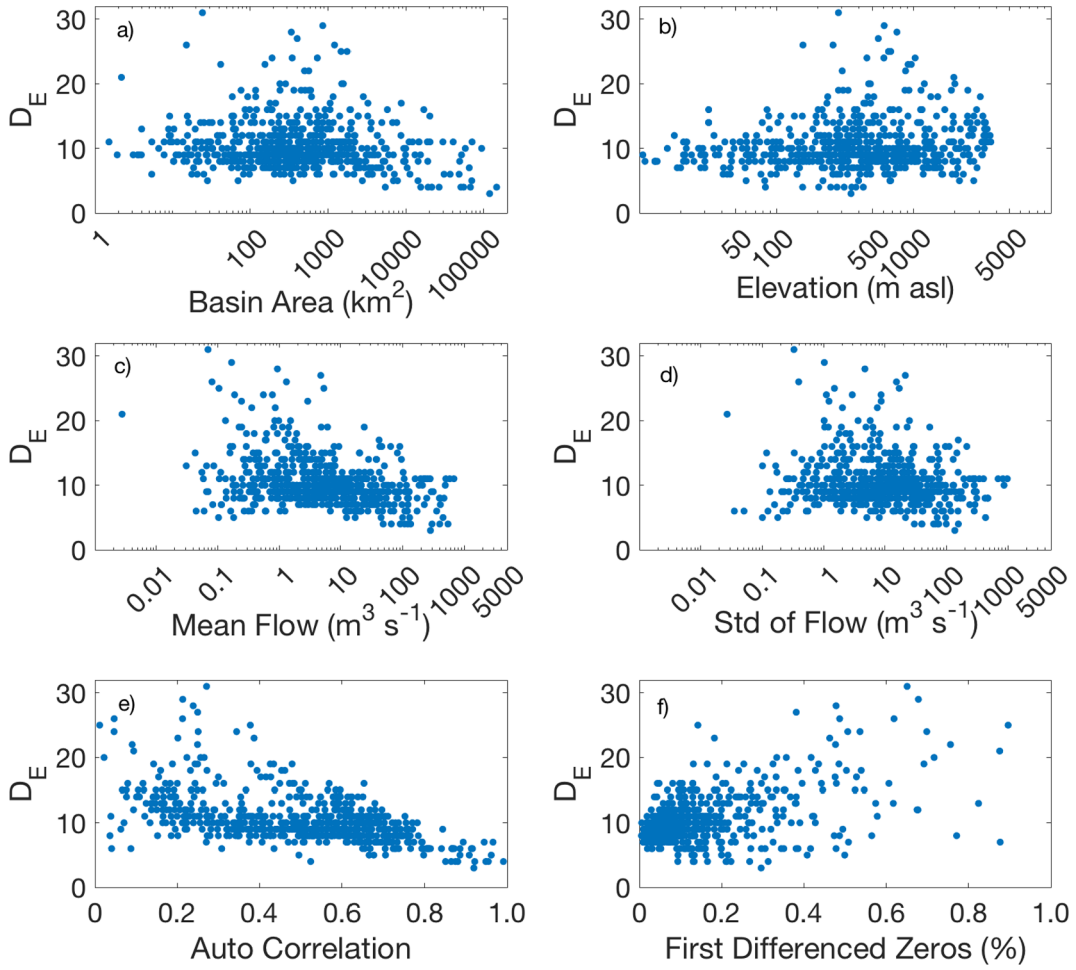

Fig. 6. The minimum embedding dimension as a function of drainage area, elevation, mean flow, and the standard deviation of flow for all the reference hydrometric sites.

is available in the Appendix Fig. A1. The spectrum of values reached its peaks primarily along the west coast and into parts of the desert southwest, as well as a region spanning portions of the Canadian Prairies and United States Great Plains southwards to the Gulf Coast of Texas and Louisiana. Similar to the findings of Vignesh et al. (2015), D_E had a slight dependence on the size of the drainage area with the lowest values of D_E only being attained from the largest basins (Fig. 6a, A5, and document supplement) but low and high values of D_E are seen across the range of basin areas and elevations. Similarly, the lowest embedding dimensions were associated with high annual mean flow (Fig. 6c), high flow variance (Fig. 6d), autocorrelation (Fig. 6e) and low first differenced zeros (Fig. 6f). While this was true for the lowest embedding dimensions, a range of low and high embedding dimensions are observed below the maximum of these ranges.

To further investigate this spectrum ofD_E, a sensitivity analysis for 37 stations along an East to West transect between the latitudes of 38.5° and 39.5° N and 24 stations along a North to South transect between 114.5° and 116.5° W was conducted. These transects are indicated as the regions bounded by red lines in Fig. 5. Regime plots, and embedding dimension (D_E) for selected stations in the East to West (Longitudinal) and North to South (Latitudinal) transects can be found in Figs. 7 and 8. Regime plots summarize the seasonal variation of streamflow showing the mean and median discharge and the 0.1 to 0.9 quantiles with the maximum and minimum values being shown as points. From the regime plots in each transect it is clear that the most snow dominated watersheds, those that exhibit large peaks in flow during spring and summer, have low embedding dimensions (e.g. Fig. 7f & g, Fig. 8c–h). Where rainfall has a seasonally consistent pattern, higher embedding dimensions are observed (Fig. 7b–d). Where the streamflow pattern has little or no seasonal structure (Fig. 7a, e & h; Fig. 8a & b) the highest embedding dimensions, greater than 13 and up to 23, were found along this transect.

3.3. Sensitivity analysis

An evaluation of the Kennel et al. (1992) FNN method as a tool to determine stream flow complexity was conducted. This involved varying the length of record investigated for all stations, and the degree of smoothing applied in preprocessing for the two transects across North America shown in Fig. 5.

3.3.1. Length of series

For the 667 stations, the length of streamflow time series varied in length from 27 to 107 years and did not appear to directly affect the embedding dimension (Fig. 9). Stations along the two transects were resampled to provide shorter records of 10–66% of the full record length. Multiple runs were analyzed for each shortened record with the start dates randomly chosen as detailed in Section 2.2. The D_E calculated from the entire time series was either within the range of values calculated or slightly greater (never more than 2 dimensions) than the range obtained from the collection of subseries. No full series values of D_E were less than the minimum value calculated for a subseries indicating complexity was never simplified when looking at a larger time window.

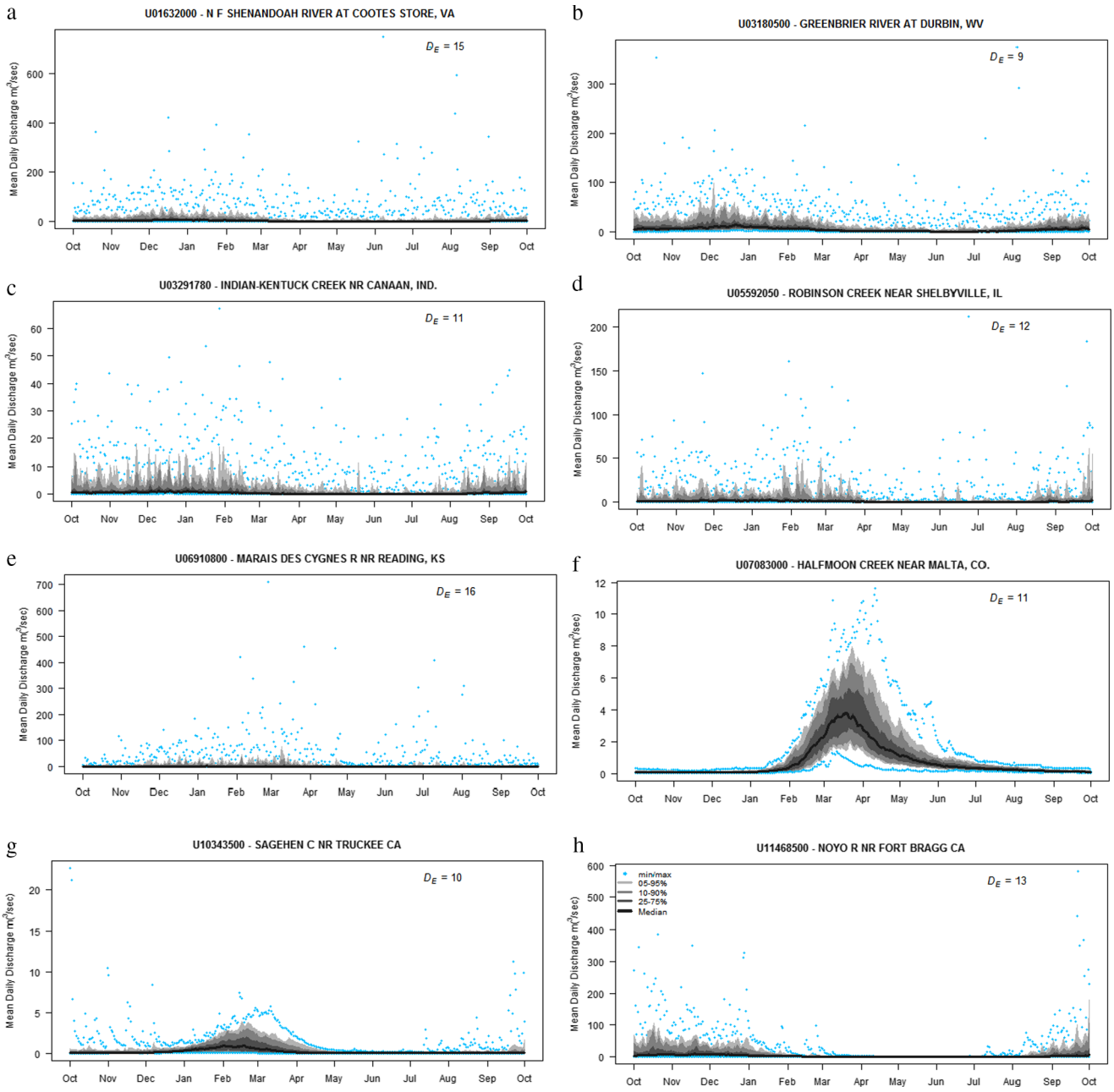

Fig. 7. Selected regime plots for watersheds from East (top) to West (bottom) from the transect shown in Fig. 5 with minimum delay embedding dimensions indicated by D_E.

It was equally likely for D_E in a pluvial or nival system to lie either within the range of subseries values or slightly above. This demonstrates that minimum embedding dimension may fluctuate around a common value or potentially increase with length. However, as indicated in Fig. 9, time series length is not a necessary nor sufficient condition for high (or low) minimum embedding dimensions. Rather, it is more likely for rivers with increasing embedding dimensions that the dynamics may evolve over time and the embedding dimension describing a longer period of the hydrological system is more complicated.

One explicit example of the sensitivity to record length is shown in Fig. 10. The embedding dimension computed for each series length is computed at 5% and 1% FNN with 5% showing fluctuations, likely related to signal noise, around a mostly steady value. The 1% threshold shows a clearer increasing trend. At 1%, D_E appears underestimated for records less than 10 years in length, and with longer records the dimension increases slightly after 45 years of data. Both cases suggest that 10 years of record may be sufficient to obtain a decent estimate of D_E and that strictly comparative estimates should have similar lengths of at least this length so as to avoid non-stationarity in embedding dimension estimates. The displayed increase in complexity with the 1% threshold may result from long term shifts in streamflow generating processes related to climate variations. This then suggests that changes in embedding dimension might be used to detect change in complexity and changes in streamflow generation, though sensitivity to such changes is dependent on the criteria for calculating D_E. Further comparisons with the 1% threshold can be found in the Appendix.

As has been indicated by many authors (e.g. Freudiger et al., 2014; McCabe et al., 2007; Vormoor et al., 2016), there have been increases of rain- and rain-on-snow-generated streamflow in mountain catchments in North America and Europe. Mountain streams in the Western United

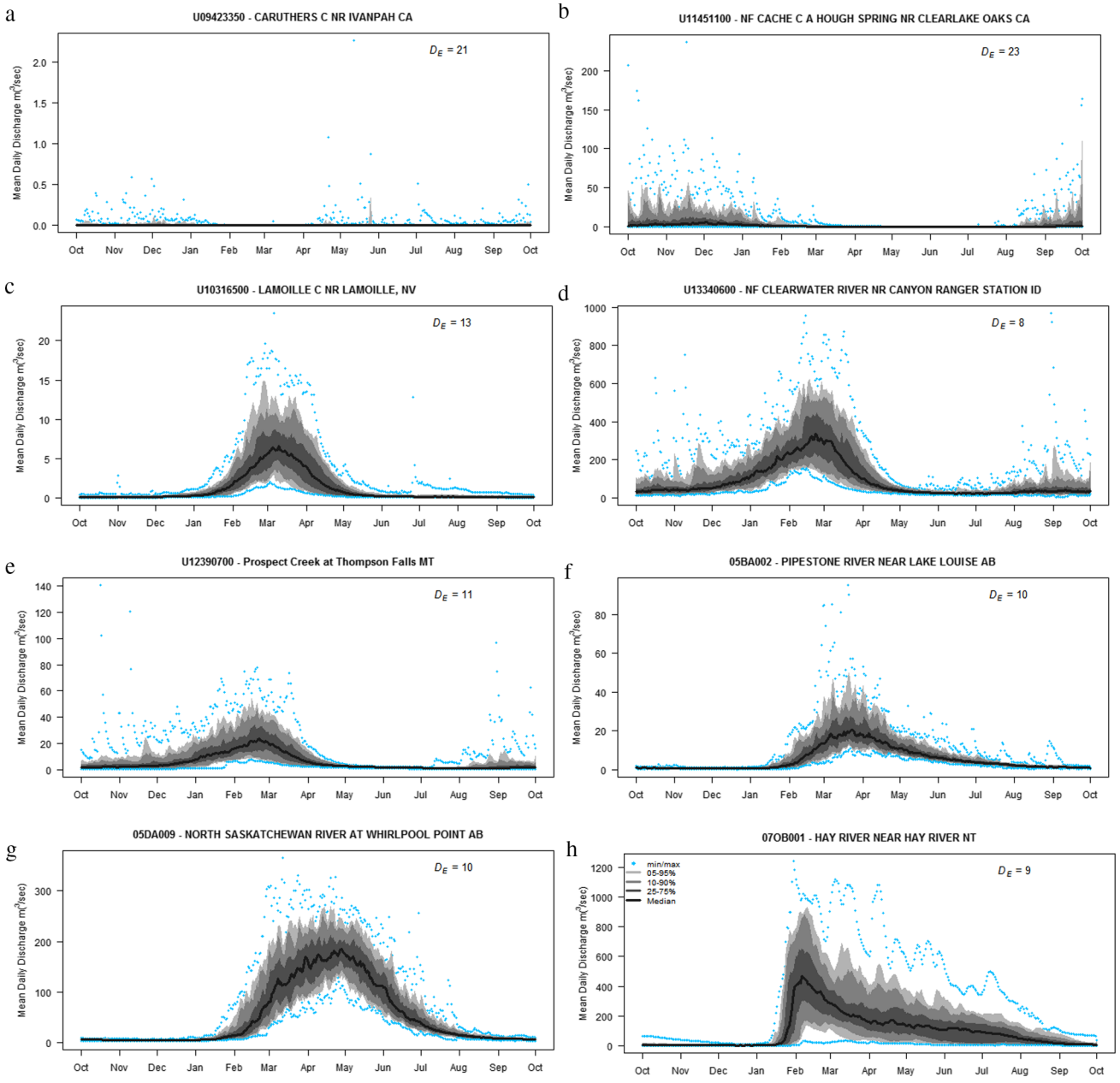

Fig. 8. Selected regime plots for watersheds from South (top) to North (bottom) from the transect shown in Fig. 5 with minimum delay embedding dimensions indicated by D_E.

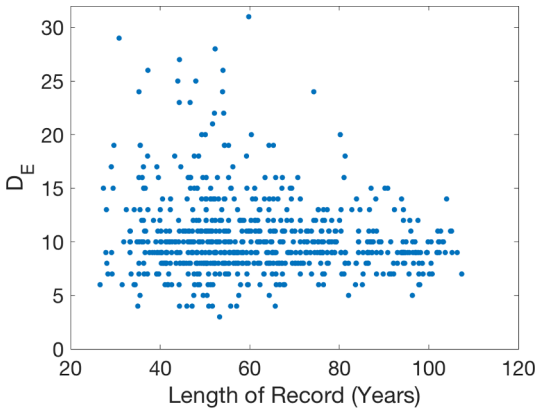

Fig. 9. Minimum embedding dimension related to length of record in years.

States with periods of record spanning more than 80 years were analyzed to see if distinct changes in 10-year-subperiod D_E values were identifiable over time. Subtle changes in hydrographs were noticed such as the Salmon River at Somes Bar, California which showed a distinct spike in D_E for the decades from 1946 to 1976. These decades coincided with some of the highest flows on record as well as multiple peak flows during single water years. As well, Lamoille Creek near Lamoille, Nevada exhibited an increase from $D_E = 12$ to $D_E = 14$ over ten-year periods spanning 1915–2015. This indicates D_E is worth future investigation as a metric for understanding hydrological regime changes and the effect of the changing climate.

3.3.2. Degree of smoothing

For both the latitudinal and longitudinal transects, increasing the sliding average window size typically decreased values of D_E, though not always monotonically. This general decreasing trend is to be expected as brief high peaks are averaged over more days and a smoother,

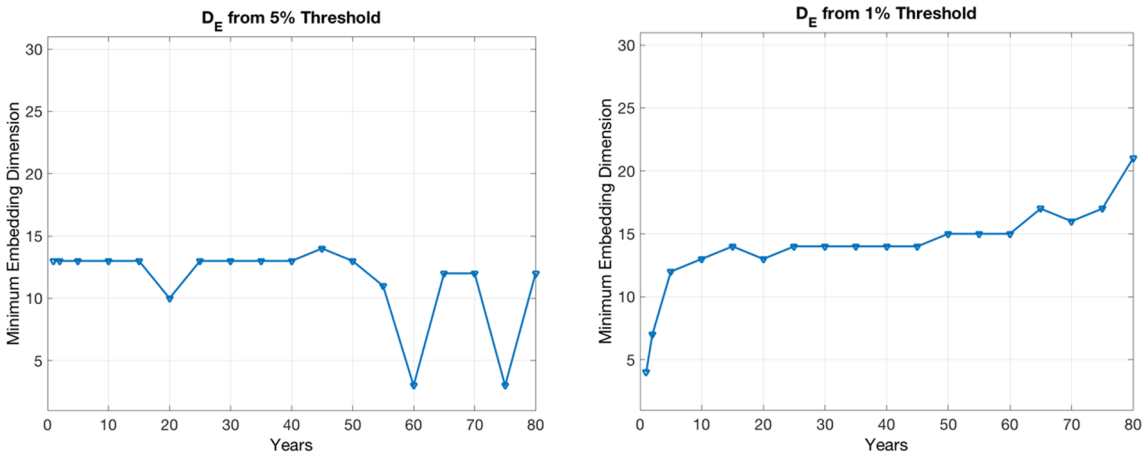

Fig. 10. An example of how record length affects the minimum embedding dimension calculated at both 5% FNN (left) and 1% FNN (right) for Lamoille Creek near Lamoille Nevada.

low-frequency fluctuating structure appears. On the pluvial end of the spectrum, smoothing had a significant effect on the Greenbrier River at Durbin, West Virginia, and Indian-Kentuck Creek near Canaan Indiana (Fig. 11a–b). Values of D_E reduced from 13 to 5, and 17 to 7, respectively when increasing smoothing from 2 days to 30. For both signals, the effect of smoothing diminished after about 10 days, though D_E continued to slowly decrease.

Some nival stations with snowmelt runoff occupying a large temporal portion of the hydrograph had a resiliency to smoothing. That is, the signal remained largely unchanged as fluctuations around the main flow structure were minimal in magnitude and smoothing negligibly affected false nearest neighbors. The annual signal of snowmelt was not considerably altered up to 30 days of smoothing. This is shown with examples of the Pipestone River near Lake Louise and the North Saskatchewan River at Whirlpool Point, Alberta in Fig. 11c and d where smoothing only decreases the embedding dimension from 10 to 7. Though the magnitude of the two streams differ by an order of magnitude, and the average peak flow differs by a month, both are driven by similar snowmelt processes on the east side of the Canadian Rocky Mountains and have nearly identical embedding dimensions for all degrees of smoothing.

Some ephemeral streams in the Southwestern United States and prairie streams with little seasonal structure did not respond with monotonically decreasing values of D_E for increased smoothing. Rather, a concave-down shape appeared. A five-year example of two such smoothed time series, Kings Creek near Manhattan, Kansas and Deep Creek near Palm Desert, California and are shown in Fig. 11a. It is worth noting that at the 1% threshold, this concave-down shape did not appear and indicates the potential over sensitivity of the 5% threshold with largely unstructured signals. As it stands, this is a topic of further investigation and indicates that excessive smoothing may have the unintended result of disregarding complex dynamics critical for describing pluvial systems.

To further compare with the results of Vignesh et al. (2015), FNN calculations were conducted using monthly mean values. The findings mimicked that of Vignesh et al. (2015) with Eastern and West coast stations obtaining the lowest embedding dimensions and mountain west stations obtaining relatively higher measures of complexity (Fig. 12). This is the inverse of what was found at daily timescales and is discussed more in Section 4. D_E values for all computation methods are available in the manuscript supplement.

4. Discussion

The embedding dimensions determined using FNN from daily streamflow provides considerable insight into streamflow dynamics across North America. Streamflow characteristics are driven by flow-generation mechanisms which are determined by the physical and biological properties of watersheds (Trancoso et al., 2018). The utility of the method is demonstrated by estimating the minimum embedding dimension, D_E, for 667 hydrological reference sites in North America and exploring the spatial distribution of D_E. Rainfall-driven and snowmelt-driven hydrological systems exhibit distinctly different embedding dimensions (Fig. 5). Low embedding dimensions are found in nival rather than in pluvial watersheds, large rather than small watersheds, at high elevation rather than low elevation watersheds, and at higher latitudes rather than low latitude watersheds. A similar study by Vignesh et al. (2015) also compared FNN dimensions of monthly streamflow to catchment characteristics and streamflow statistical properties. Low embedding dimensions occurred at both low and high elevations in both studies, but Vignesh et al. (2015) suggests that high values are predominant at low elevations. This is not the case with the present study where the highest elevations were associated with lowest values of D_E, but the lowest elevations also had low values. In both studies, high embedding dimensions were associated only with lower mean flows (Fig. 6). Standard deviation of flow appears to be a weak measures of streamflow dynamics as there was no positive relationship with D_E, in contrast to Vignesh et al. (2015). It is clear that at the extremes of these explanatory variables there is some clarity, but for each of these variables low and high embedding dimensions are obtained across most of the range.

Porporato and Ridolfi (2003) present a state-space method reconstruction of a streamflow time series using nonlinear methods such as those proposed by Abarbanel et al. (1993). Porporato and Ridolfi (2003) detected low-dimensional nonlinear components and dynamics and deterministic and nonlinear components on longer time scales when glaciers and snowmelt contribute to streamflow. This is the case in the present work, low embedding dimensions are associated with the

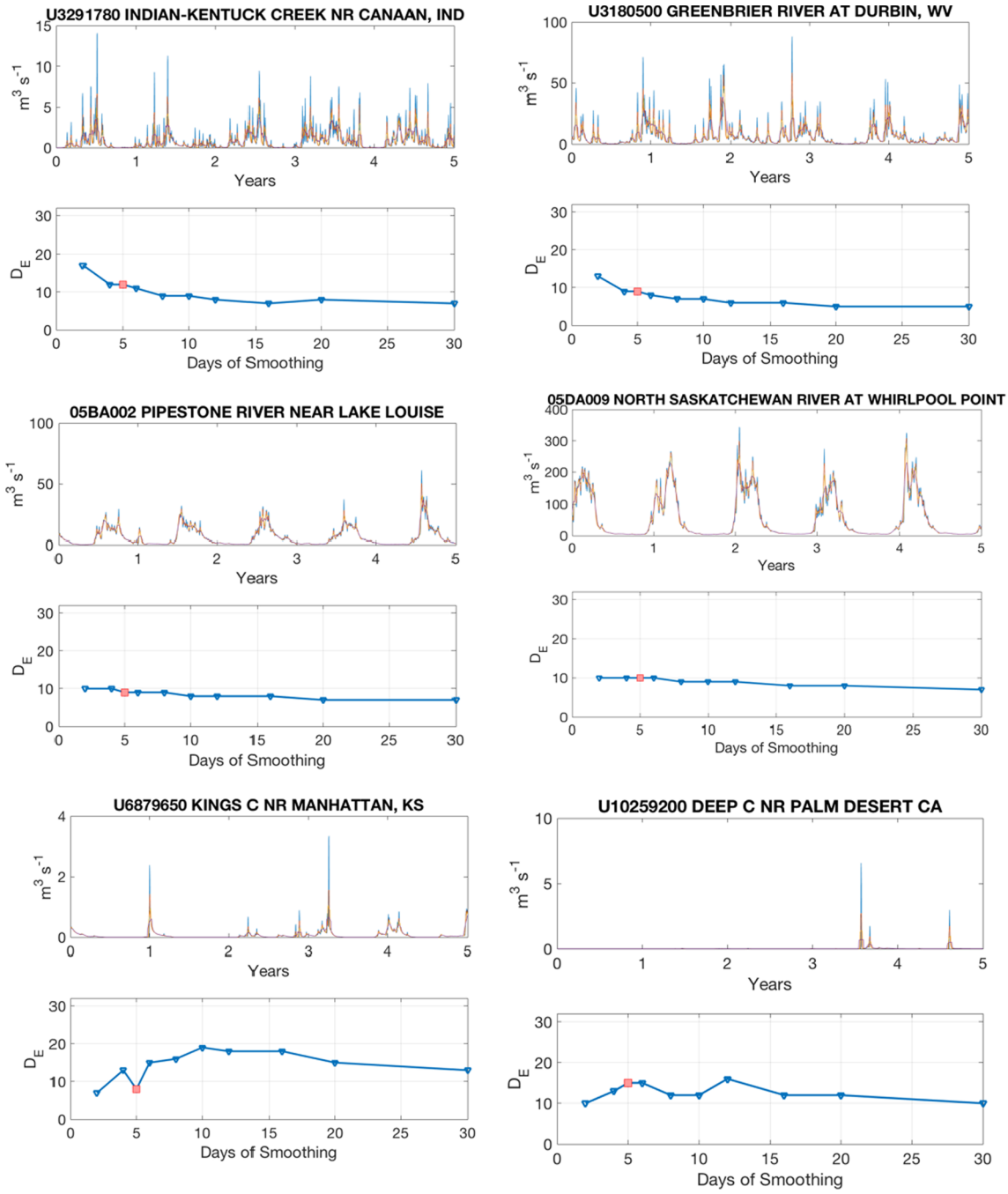

Fig. 11. Variable smoothing and the effect on minimum embedding dimension for 6 rivers in the North to South and East to West transects. The upper panel in each shows a five-year period of two, five-, ten-, and twenty-day averaged streamflow. The lower panel in each shows the values of D_E from 5 days of smoothing are indicated with a red box in the lower subplots. (For interpretation of the references to color in this figure legend, the reader is referred to the web version of this article.)

predominance of snowmelt as a generating process, and higher dimensions associated with seasonal or more random rainfall patterns.

At high embedding dimensions, FNN failed for Vignesh et al. (2015), but this was not the case for our study, even for cases that were non-convergent cases using a 1% threshold (Appendix). This is likely a difference in the codes used as they report that they followed the same geometric method of Kennel. This is also potentially a good indicator that their method was not overly resistant to noise. It might also be a reason why they used monthly data and minimum D_E values instead of a threshold.

Abarbanel et al. (1993) suggest that a 1% FNN threshold is sufficient for physicists interested in the dimension of dynamical systems. For 14% of the cases considered here, the %FNN never falls below the 1% used in Abarbanel et al. (1993) (see Appendix for details). Other studies have avoided this problem by using correlation dimension instead of the %FNN technique (Sivakumar et al., 2015) or simply using the embedding dimension of the lowest %FNN (Vignesh et al., 2015). Correlation dimensions also resulted in some rivers to be "unidentifiable" (Sivakumar et al., 2015). In contrast to the %FNN plots of Vignesh et al. (2015), there was a general decrease in %FNN with increasing

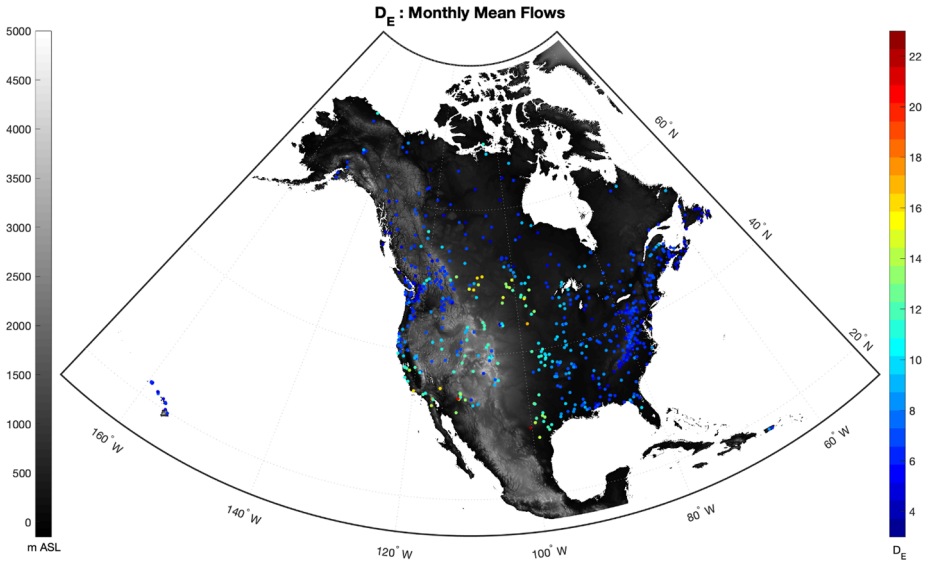

Fig. 12. Minimum embedding dimensions calculated using mean monthly US streamflow values instead of daily flow as in Fig. 5. Note the inverse relationship with values found in Fig. 5 in the Mountain West and Great Plains regions. The underlying grayscale map shows topography.

embedding dimension, even for the non-convergent cases (Figs. A2,3). The reality might be that 1% is too strict for dealing with streamflow time series and we have used a 5% threshold here as 95 cases did not reach the 1% threshold by $D_E = 30$. There is a tradeoff as at 5% as D_E computations are less stable and more sensitive to varying signal length and smoothing (e.g. Fig. 10, 11e–f).

False nearest neighbor algorithms are invariant under linear translations and rescaling (e.g. subtracting means and dividing by standard deviations). Additionally, Abarbanel et al. (1993) demonstrated that the addition of uniform noise does not affect the embedding dimension. In the Lorenz and synthetic streamflow example, the amount of white noise added affects the embedding dimension (Fig. 2b), but does so by affecting the percentage of false nearest neighbors in random subseries. This sort of process in nature may have resulted in the threshold of 1% being too low as is evident in Fig. 2b (and Figs. A1 and A3).

Synthetic data were used to explore several aspects of the determination of embedding dimension. Synthetic time series that mimic snowmelt, rainfall and noise contributions to time series allow the embedding dimension to be explored in some detail to demonstrate that embedding dimension provides information about separation of these two processes. The results from embedding dimensions on synthetic data show that the embedding dimension is lowest when dominated by a fixed-period snowmelt signal and highest when dominated by a random rainfall signal (Fig. 3, Fig. 4a). The simulations showed that this change in dimension was quasi-linear when only two signals contributed to the embedding dimension, but the embedding dimensions obtained were much lower that with real streamflow time series which are obviously more complex (Fig. 4a). That the embedding dimension changes when the ratio of snowmelt to rainfall changes suggests that embedding dimension might be used to assess dynamic structure that changes over time either due to linear trends or climate system variability. Future work may lead to methods that approach measuring these changes more directly than current linear methods that try to demonstrate shifts in timing related to changes in generating processes (Burn and Whitfield, 2017, 2018a,b).

Smoothing and the choice of a time delay are important considerations of the FNN method. We used daily data with a five-day smoothing, based upon a desire to make fair comparisons between large and small basins; Whitfield (1998) showed that the information content of small and more pluvial watersheds were more information rich than large snowmelt driven watersheds. The five-day smoothing reduces the difference without over-smoothing. The mapping of D_E that Vignesh et al. (2015) provide for embedding dimensions for monthly data is qualitatively the opposite pattern to that presented in our Fig. 5. By mapping FNN embedding dimension, Vignesh et al. (2015) demonstrate differences in variability in streamflow dynamics across the US; lower delay times result in wider variability in the embedding dimension in the west than in the east. Fig. 5 shows the results from our method, daily streamflow smoothed to 5 days, 5% threshold and an AMI-based time delay. This plot is markedly different to that presented in Vignesh et al. (2015). Using mean monthly data, a 5% threshold and the same AMI-based time delay we obtain a result (Fig. 12) that is similar to Fig. 3 provided in Vignesh et al. (2015). The main differences between the generation of the two figures is that we use a 5% threshold and they use of the embedding dimension of the minimum number of false nearest neighbors, based upon five different delay times. The dataset is also not identical, though both sets of US data come from the US reference hydrological network. The differences between Fig. 5 and Fig. 12 (and to Fig. 3 of Vignesh et al. (2015)) are due to the use of monthly data rather than smoothed daily data.

Some of the relationships between D_E and physical or statistical measures of streamflow were similar to those that Vignesh et al. (2015) had obtained using monthly data, although Vignesh et al. (2015) found low embedding dimensions occur in both small and large drainage basins and (relatively) high embedding dimensions are associated only with small drainage areas. Our contention would be that while some smoothing of a daily streamflow series is necessary to deal with the basic issues of more information being present in small rainfall driven watersheds to make fair comparisons with larger or snowmelt-driven systems, the amount of smoothing should be small since over-smoothing over-simplifies the short time-scale dynamics driving streamflow, as mentioned above. With the exception of Khatibi et al. (2012) who also used daily data, all of the other papers we have cited use monthly data. Our view would be that the use of monthly data over-smooths the short timescale dynamics and leads to incorrect results.

The sensitivity studies presented here demonstrate that a sufficient length of series is necessary, but this length is short (~10 years in Fig. 10) and increasing the length beyond this has no consistent effect

between rivers. We found no relationship between embedding dimension and total record length (Fig. 9). When considering long-term temporal changes, such as those related to changes in climate and runoff generating processes, a reasonable length of record is still needed to estimate an embedding dimension and to also allow multiple measurements of the dimension to be made over time. We have demonstrated that embedding dimension does respond to changes in complexity over time in simple experiments with synthetic data (Fig. 4a). The sensitivity studies limited themselves to daily time steps; it would be useful to extend the studies to smaller time steps to capture diel scale or finer processes. Finding such clear relationships in nature was more difficult and suggests further refinement of such a technique is necessary. Further development could complement Maskey et al. (2016) who used a deterministic fractal-multifractal approach to identify fractal parameters in streamflow time series and showed that the time evolution of the parameters is useful for tracking and predicting change in streamflow generating processes. Future work should also consider how combinations of processes contribute to the complexity as such information would be useful in determining simulation model structure and for assessing changes over time particular where the relative contributions of processes change or processes are added or removed.

We examined the streamflow pattern from stations along two transects shown in Fig. 5. Stations from the East to West transect are shown in Fig. 7, and from the South to North transect are shown in Fig. 8. Along both transects, the sites with the lowest embedding dimensions have strong snowmelt signatures; where the variability in timing and magnitude of peak flows is lowest, at high latitude and/or high elevation, the embedding dimensions are lowest. Peterson et al. (1987) examined the hydrology of a north-south transect of the west coast of North America. Trancoso et al. (2018) examined how the biophysical properties from 354 catchments across a climatic gradient in Australia contributed to hydrological attributes. Transects across a gradient, or as in our case, multiple gradients provide a useful check on the structure of results. In Figs. 7 and 8, there are clear progressions in both embedding dimension and structure of the hydrograph related to the physical environments encountered along the transects.

Many classification systems fail because they do not simultaneously deal with hydrograph shape, magnitude and timing. As examples, Hannah et al. (2005) showed classification of hydrographs using shape and magnitude; Fleming et al. (2007) showed that differences in latitude or elevation resulted in temporal shifts that place hydrographs generated by the same processes into different classes because of timing differences. These are artifacts of using linear methods where nonlinear methods would be preferable. In Figs. 5, 7 and 8 it is clear that embedding dimension shows differences that are related to process differences and not simply temporal and magnitude shifts.

Sivakumar et al. (2007) argue on behalf of a globally accepted classification system for hydrology. While we agree that a classification system in hydrology is desirable, most classification systems place items in subjective bins based upon specific criteria. Sivakumar and Singh (2012) used correlation dimension of 117 stations in the United States to create a four-level classification (low, medium, high and unidentifiable). Their classification shows some homogeneity within some regions but contained strong exceptions. This supports the suggestion of Burn and Whitfield (2017) that discrete hydrologic regimes are an artificial construct and that the processes should be considered along a continuum. Sivakumar et al. (2015) stress the need for a measurement of system complexity as a basis for a classification framework and identified the potential for nonlinear dynamics and other recent concepts of complex systems for assessing complexity. Sivakumar et al. (2007) considered classification from a phase space perspective and building a classification based upon complexity. Sivakumar et al. (2007) report attractors ranging from very clear to very blurred.

The embedding dimension results presented here and elsewhere suggest that hydrologic dynamics fall across a continuum and formal bins would not be appropriate. The many mechanisms that govern river flow dynamics are expressed across a wide range of temporal and spatial scales (Porporato and Ridolfi, 2003). Porporato and Ridolfi (2003) report that the distinction between linearity and nonlinearity as a function of discharge becomes more precise as the attractor is better unfolded only at higher embedding dimensions (up to $m = 9$). While the present research did not focus on the existence of attractors, we have demonstrated that embedding dimension is a useful measure for quantifying the pluvial-nival continuum when estimated to much higher dimensions. Future work should also consider how combinations of processes contribute to the complexity, as such information would be useful in determining simulation model structure and for assessing temporal changes where proportions of process contributions change or processes are added or removed. Similarly, the methods may be also applied to other situations such as changing land use and urbanization within watersheds.

Considering high-dimensional descriptions of these streamflow processes as meaningful information, and not the effect of meaningless noise, is consistent with the theory that weather systems are unlikely to be able to represented at low-dimensions (Lorenz, 1991; Abarbanel et al., 1993; Abarbanel and Lall, 1996). Many of the pluvial rivers display high-frequency dynamics and high embedding dimensions, likely only represented at the weather system scale. Furthermore, some ephemeral streams, such as Deep Creek (Fig. 11), respond directly to weather systems, and only once every few years, a return period that may be influenced by climate. This degree of complexity should be considered before accurate representations of climate-change in these hydrological systems are expected to be representable.

The necessity of a better understanding of the distinguishing factors of pluvial and nival rivers in changing climate has increased (Burn and Whitfield, 2017). If warming causes a shift to pluvial processes from nival processes, more frequent rain-on-snow and rainfall driven floods may result (Burn and Whitfield, 2017; Whitfield et al., 2012). While nonlinear processes are common in hydrology, the use of nonlinear methods is less so. The mathematically rigorous procedures that can be used to examine the real-world dynamics from time series that appear to be highly variable, complex, and often random (Huffaker et al., 2017), such as was demonstrated here, may improve our ability to understand watershed hydrological processes and diagnose change from streamflow time series. While the difficulty of the methods remains a barrier (Dooge, 1986); recent developments, including the examples presented here, suggest this is an area with great promise.

5. Conclusions

A nonlinear False Nearest Neighbor approach was used to determine the minimum embedding dimension of 667 streamflow time series from reference hydrological stations across Canada and the United States including Alaska, Hawaii and Puerto Rico. Low embedding dimensions are found in cold areas at higher elevations and latitudes with strongly periodic snowmelt signals. High embedding dimensions are associated with rainfall and less periodic (more stochastic) runoff patterns. This suggests that embedding dimension is a useful measure of location on a previously-hypothesized pluvial-nival continuum (Burn and Whitfield, 2016, 2017), and that high dimensions may actually be indicative of complex underlying physics, not purely noise. Further investigation explaining the influence of specific noise-generating processes in environmental studies would benefit future users of this method.

Sensitivity investigations demonstrate that a streamflow time series of about 10 years duration may be sufficient to obtain a comparatively meaningful estimate of the embedding dimension. Low embedding

dimension is associated with high latitude, high and low elevation and large watersheds. These are predominantly nival watersheds. Higher embedding dimensions are associated with smaller watersheds, low elevations and low latitudes. Coastal areas of North America, Hawaii and Puerto Rico have higher embedding dimensions. When using a 1% threshold for FNN, some watersheds did not converge; using a 5% threshold is perhaps more appropriate for streamflow time series as it reduced the number of non-convergent cases.

Reinterpreting high embedding dimensions as valuable information, instead of smoothing for simpler results, actually expands our working framework to allow for weather-driven systems that have been known to be very high (or infinite) dimension and follows the suggestion of Lorenz (1991). Synthetic time series were used to demonstrate that embedding dimension captures the role of the mixture of rainfall and snowmelt in a streamflow time series. Synthetic time series result in lower embedding dimension than real streamflow series because they are less complex. Varying the mixture of snowmelt to rainfall over a long time series demonstrated that the embedding dimension can be used to diagnose changes over time in a single series. The nonlinear FNN technique used here quantifies and accounts for hydrological processes that are highly variable, complex, and often random. The differences in embedding dimension illustrate the relative position on the pluvial-nival continuum and reflect the differences in complexity of these systems. Changes in the embedding dimension of the streamflow time series over time are expected to provide insight to changes in streamflow generating processes that result from climate variations, global warming, and land use change.

Declaration of interests

None.

Acknowledgments

The streamflow time series used in this study were obtained from the Water Survey of Canada and United States Geological Survey web portals. We would also like to thank John Pomeroy for his comments and suggestions, and for financial support from his grants from the Canada Research Chairs Programme, NSERC, and Alberta Environment and Sustainable Development. The comments and suggestions from two reviewers were helpful in preparing the final manuscript. The authors declare no conflict of interest.

Appendix

Abarbanel et al. (1993) suggest that a 1% threshold of false nearest neighbors should be adequate for physics applications, though hydrological data contains considerable noise with many compounding physical processes. Fig. A1 shows the spatial map of embedding distances obtained using a 1% threshold with non-convergence indicated with a value of $D_E = 31$. Values ranged from 4 to the maximum dimension we allowed (30). Non-convergence is prevalent in Vignesh et al. (2015), and they addressed this issue by using the first dimension at which %FNN reaches its minimum instead of a percent threshold. Sivakumar and Singh (2012) considered those that did not converge to be unidentifiable. The results obtained with the 1% threshold proposed by Abarbanel et al. (1993) are shown here and indicate that 5% may be a reasonable compromise for streamflow time series. Most of the non-convergent sites at 1% appear as high D_E sites at 5%, indicating a high level of complexity was detected at both thresholds.

The non-convergent watersheds are investigated in this appendix to address potential future improvements on the application of delay em-

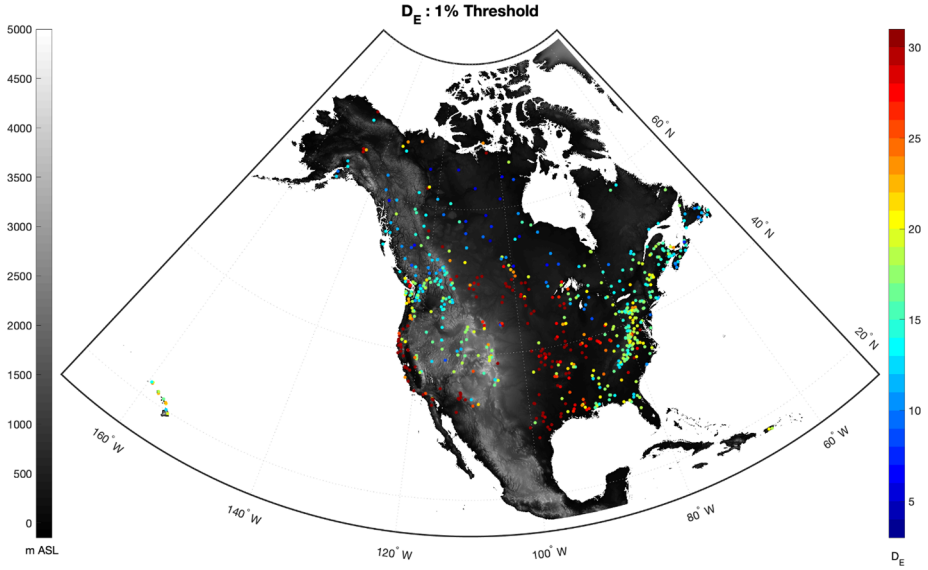

Fig. A1. Minimum delay embedding dimensions for streams across USA and Canada as calculated with the Kennel et al. (1992) false nearest neighbor algorithm and an FNN threshold of 1%.

bedding dimensions to better understand streamflow dynamics. The amount low- or no-flow conditions in non-convergent streams is examined in Fig. A2. Each non-convergent watershed was binned into a 2% wide bin according to the temporal percent of no streamflow (Fig. A2 top) or < 1% mean streamflow (bottom). The histograms indicate that while there is a higher proportion of non-convergent watersheds with long low- or no-flow periods as compared to the total sample set, there are still 30% of non-convergent sites that have < 2% of no-flow in the entire time series. Similarly, 18% of non-convergent watersheds had < 2% low-flow in their entire time series. This suggests that while periods of low-flow are often present in high dimensional watersheds, it is not a necessary condition for large D_E.

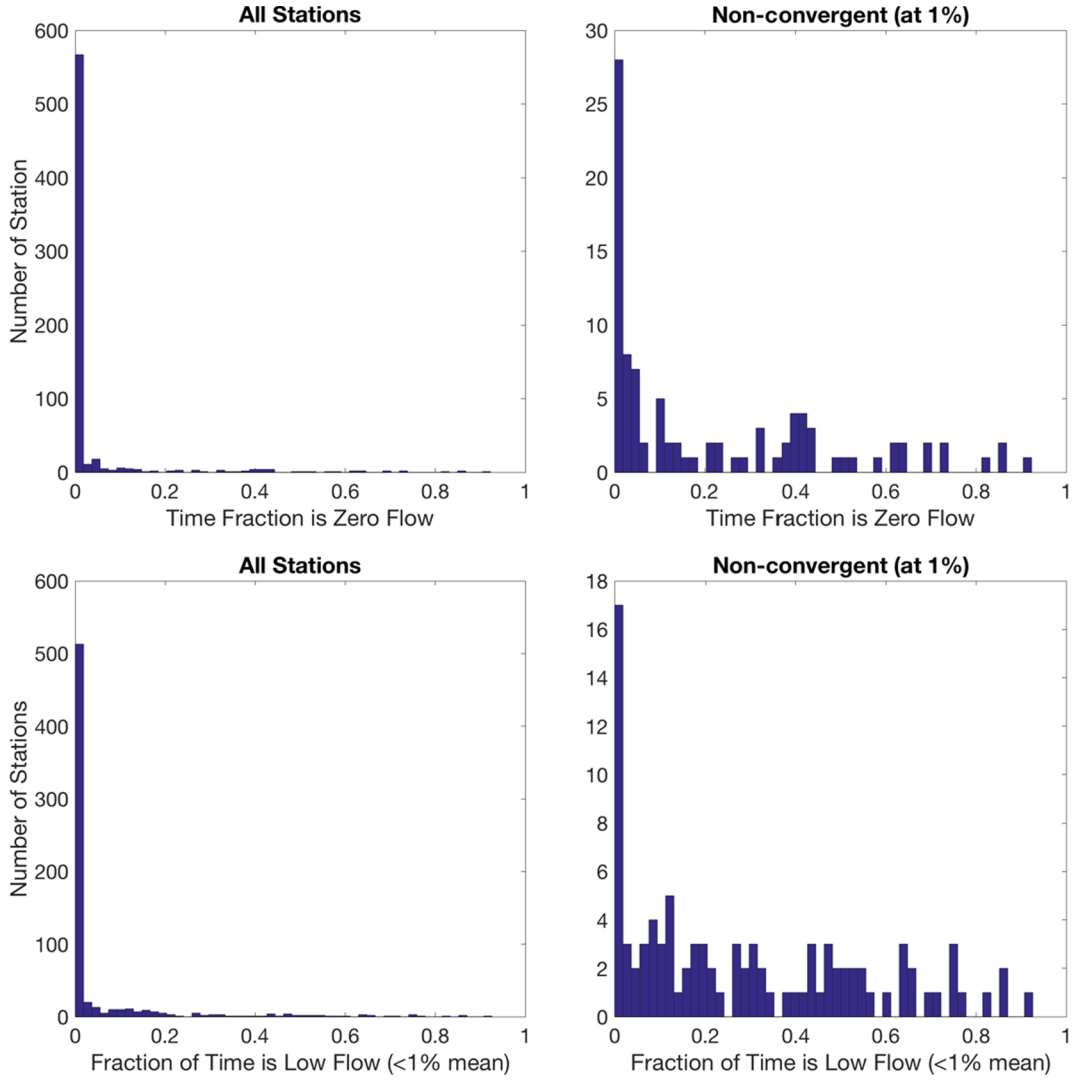

Fig. A2. Histograms of the numbers of stations with temporal fraction of zero flow (top row) and low flow (< 1% mean streamflow). All stations are considered in the left plots and only the 95 non-convergent stations are considered on the right.

This can be understood as a recurrent low- or no-flow season forces time series embedding returns to a periodic point that is a 0-dimensional subset in the delay embedding space. This was also the case for the synthetic pure snowmelt signal in Section 3.1 Instead, it is actually the irregularity of the "on-off" signal that increases the complexity of the signal, and continues to generate false nearest neighbors, thus forcing a higher embedding dimension. In hydrology, this could be manifested by irregular rain events (as seen above), variable snowmelt runoff, or multiple snowmelt peaks, among other processes.

In Fig. A3 we show the results for the 95 cases that never reached the 1% threshold and were considered non-convergent. The positive direction

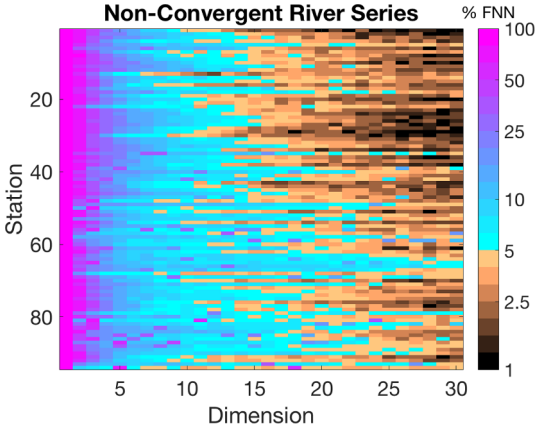

Fig. A3. Embedding dimensions to 30 for all non-convergent stations. Coloring is percent FNN greater than or equal to 1%.

on the horizontal axis represents increases in embedding dimension, and the raster plot shows a decreasing trend in %FNN for all watersheds. When the %FNN falls below a 5% threshold, the colormap transition to a brown color scheme for clarity. Some cases fall below the 5 and 10% thresholds atD_E = 5 or 6, while only one still fails to converge by an embedding dimension of 30. It is worth noting that this river (Dry Creek at Union City, California) converged at D_E = 50 and was largely ephemeral, containing 65% no-flow.

In Fig. A4 we show the decreasing %FNN for 10 non-convergent stations selected at random to show that some of these stations reach a minimum, without that minimum being below the 1% threshold. Five-year periods of streamflow for these 10 rivers are displayed in the lower subplots of Fig. A4. The majority of the rivers show complex irregular rain-fall influenced dynamics, but an irregular snowmelt signal in British Columbia, Canada is also presented (Fig. A4j), showing snowmelt alone does not guarantee low embedding dimension.

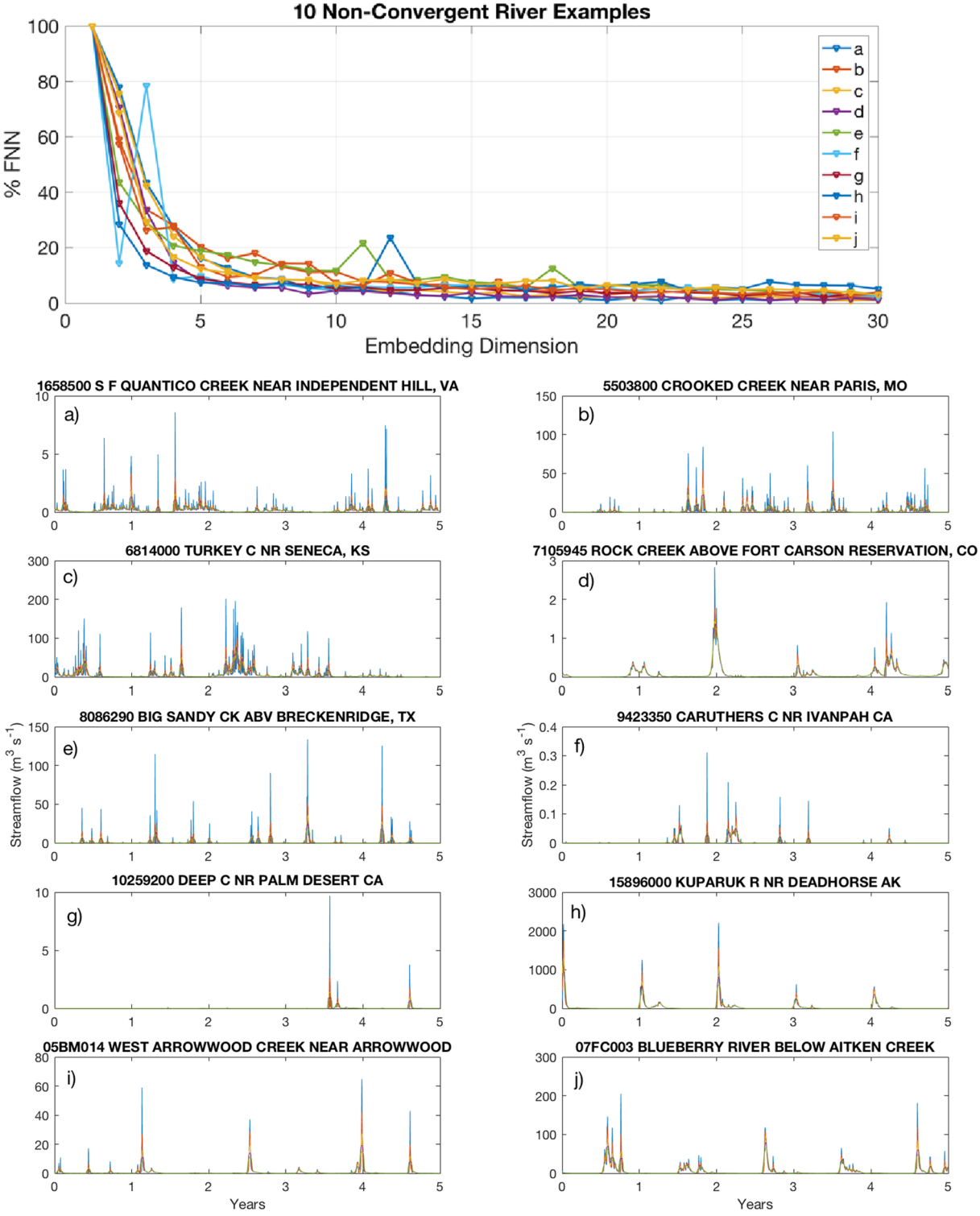

Fig. A4. Top Plot: Percent False Nearest Neighbors and embedding dimensions for 10 stations in Fig. A3 that did not converge below the 1% threshold. Subplots a–j: 5-year time series of corresponding non-convergent stream flows. Each signal shows varying degrees of smoothing. Lower subplot labels correspond with lines in top subplot.

Abarbanel et al. (1993, Figure 17) and our Fig. 2b show that noise in the streamflow record would not affect the embedding dimension, but would affect the threshold that can be achieved. One technique to address high values of %FNN may be the cleaning technique as suggested by Abarbanel et al. (1993). As many of the non-convergent time series in the present work contain periods with zero discharge, exploring this issue is a subject for future investigations. A reasonable compromise of a 5% threshold (instead of the 1% Abarbanel et al. (1993)) may appropriately account for the dynamics and noise present in streamflow signals.

The corresponding relationships between D_E, basin characteristics and streamflow statistics with this threshold can also be found in that plot (Fig. A5). Note that the scatter plots effectively show the same patterns as Fig. 6.

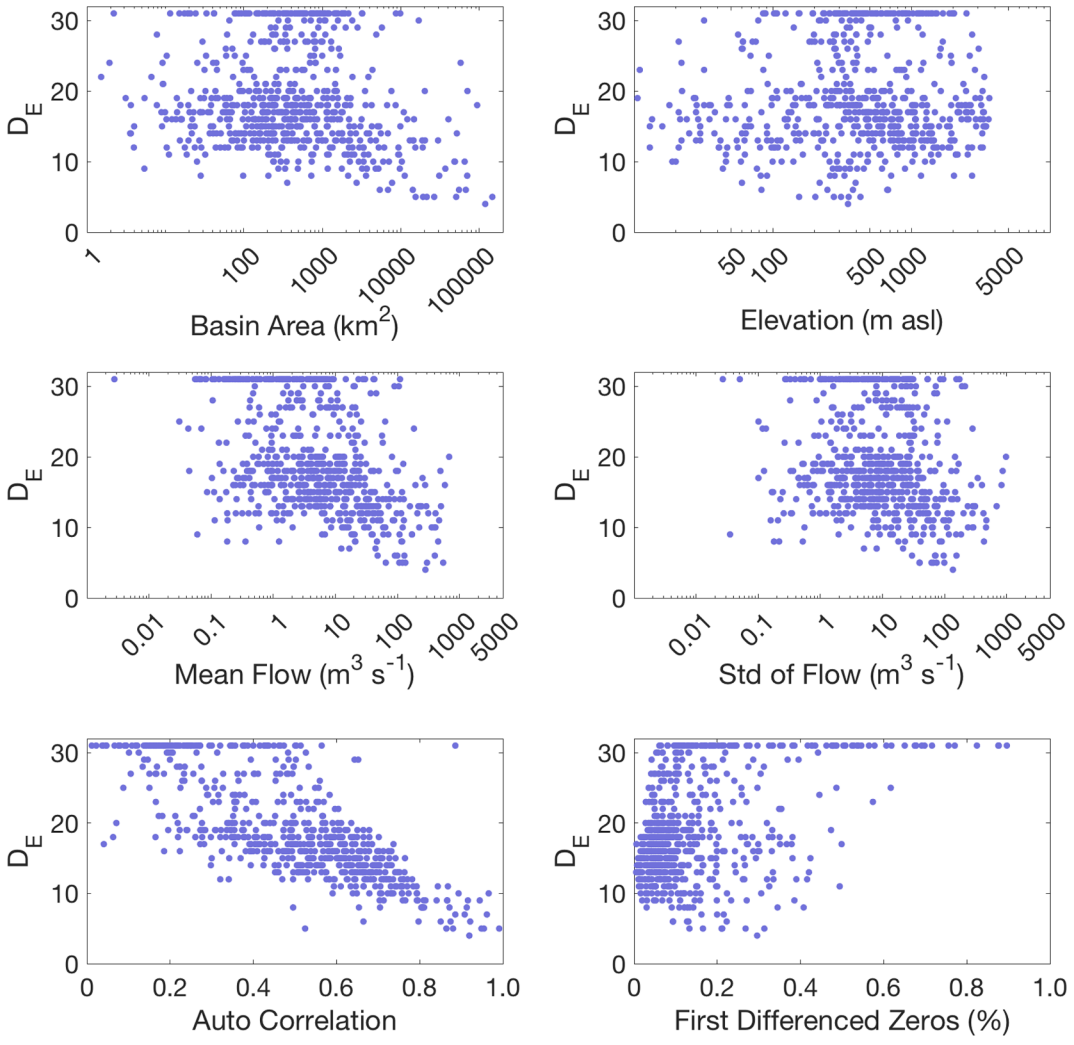

Fig. A5. Versions of Fig. 6 prepared using a threshold of 1% for False Nearest Neighbors.

References

Abarbanel, H.D.I., Lall, U., 1996. Nonlinear dynamics of the Great Salt Lake: system identification and prediction. Clim. Dyn. 12 (4), 287–297.

Abarbanel, H.D.I., Lall, U., Moon, Y.-I., Mann, M.E., Sangoyomi, T., 1996. Nonlinear dynamics and the Great Salt Lake: a predictable indicator of regional climate. Energy 21 (7–8), 655–665.

Abarbanel, H.D.J., Brown, R., Sidorovich, J.J., Tsimring, L.S., 1993. The analysis of observed chaotic data in physical systems. Rev. Mod. Phys. 65 (4), 1331–1392.

Amorocho, J., 1963. Measures of the linearity of hydrologic systems. J. Geophys. Res. 68 (8), 2237–2249.

Amorocho, J., 1967. The nonlinear prediction problem in the study of the runoff cycle. Water Resour. Res. 3 (3), 861–880.

Arnell, N.W., Gosling, S.N., 2013. The impacts of climate change on river flow regimes at the global scale. J. Hydrol. 486, 351–364.

Burn, D.H., Whitfield, P.H., 2016. Changes in floods and flood regimes in Canada. Can. Water Resour. J. 41, 139–150.

Burn, D.H., Whitfield, P.H., 2017. Changes in cold region flood regimes inferred from long record reference gauging stations. Water Resour. Res. https://doi.org/10.1002/2016WR020108.

Burn, D.H., Whitfield, P.H., 2018a. Changes in flood events inferred from centennial length streamflow data records. Adv. Water Resour. https://doi.org/10.1016/j.advwatres.2018.08.017.

Burn, D.H., Whitfield, P.H., 2018 in press. Changes in flood events inferred from centennial length streamflow data records. Advances in Water Resources. doi: 10.1002/2016WR020108.

Coopersmith, E.J., Minsker, B.S., Sivapalan, M., 2014. Patterns of regional hydroclimatic shifts: An analysis of changing hydrologic regimes. Water Resour. Res. 50, 1960–1983.

Coulibaly, P., Baldwin, C.K., 2005. Nonstationary hydrological time series forecasting using nonlinear dynamic methods. J. Hydrol. 307 (1–4), 164–174.

Dooge, J.C.I., 1986. Looking for hydrologic laws. Water Resour. Res. 22 (9S).

Fleming, S.W., Whitfield, P.H., Moore, R.D., Quilty, E.J., 2007. Regime-dependant streamflow sensitivities to Pacific climate modes across the Georgia-Puget transboundary ecoregion. Hydrol. Process. 21, 3264–3287.

Freudiger, D., Kohn, I., Stahl, K., Weiler, M., 2014. Large-scale analysis of changing frequencies of rain-on-snow events with flood-generation potential. Hydrol. Earth Syst. Sci. 18 (7), 2695–2709.

Hannaford, J., Buys, G., 2012. Trends in seasonal river flow regimes in the UK. J. Hydrol. 475, 158–175.

Hannah, D.M., Kansakar, S.R., Gerrard, A.J., Rees, G., 2005. Flow regimes of Himalayan

rivers of Nepal: nature and spatial patterns. J. Hydrol. 308, 18–32.
Hannah, D.M., Smith, B.G.P., Gurnell, A.M., McGregor, G.R., 2000. An approach to hydrograph classification. Hydrol. Process. 14 (2), 317–338.
Huffaker, R., Bittelli, M., Rosa, R., 2017. Nonlinear Time Series Analysis with R. Oxford University Press, Oxford, UK, pp. 360.
Kantz, H., Schreiber, T., 2003. Nonlinear Time Series Analysis. Cambridge University Press, Cambridge UK, pp. 388.
Kennel, M.B., 1997. Statistical test for dynamical nonstationarity in observed time-series data. Phys. Rev. E 56 (1), 316.
Kennel, M.B., Brown, R., Abarbanel, H.D.I., 1992. Determining embedding dimension for phase-space reconstruction using a geometrical construction. Phys. Rev. A 45 (6), 3403.
Khatibi, R., et al., 2012. Investigating chaos in river stage and discharge time series. J. Hydrol. 414, 108–117.
Kostelich, E.J., Yorke, J.A., 1990. Noise reduction: finding the simplest dynamical system consistent with the data. Physica D: Nonlinear Phenomena 41 (2), 183–196.
Lall, U., Mann, M., 1995. The Great Salt Lake: a barometer of low-frequency climatic variability. Water Resour. Res. 31 (10), 2503–2515.
Lall, U., Sangoyomi, T., Abarbanel, H.D.I., 1996. Nonlinear dynamics of the Great Salt Lake: Nonparametric short-term forecasting. Water Resour. Res. 32 (4), 975–985.
Lorenz, E.N., 1991. Dimension of weather and climate attractors. Nature 353, 241–244.
Mann, M.E., Lall, U., Saltzman, B., 1995. Decadal-to-centennial-scale climate variability: insights into the rise and fall of the Great Salt Lake. Geophys. Res. Lett. 22 (8), 937–940.
March, T.K., Chapman, S.C., Dendy, R.O., 2005. Recurrence plot statistics and the effect of embedding. Physica D 200, 171–184.
Marwan, N., Romao, M.C., Theil, M., Kurths, J., 2007. Recurrence plots for the analysis of complex systems. Phys. Rep. 438, 237–329.
Maskey, M.L., Puente, C.E., Sivakumar, B., 2016. A comparison of fractal-multifractal techniques for encoding streamflow records. J. Hydrol.
McCabe, G.J., Clark, M.P., Hay, L.E., 2007. Rain-on-snow events in the western United States. Bull. Am. Meteorol. Soc. 88, 319–328.
Peterson, D.H., Cayan, D.R., DiLeo-Stevens, J., Ross, T.G., 1987. Some effects of climate variability on hydrology in western North America, The Influence of Climate Change. In: and Climatic Variability on the Hydrologic Regime and Water Resources (Proceedings of the Vancouver Symposium, pp. 45–62.
Porporato, A., Ridolfi, L., 2003. Detecting determinism and nonlinearity in riverflow time series. Hydrol. Sci. 48, 763–780.
Sangoyomi, T.B., Lall, U., Abarbanel, H.D.I., 1996. Nonlinear dynamics of the Great Salt Lake: dimension estimation. Water Resour. Res. 32 (1), 149–159.
Schertzer, D., Tchiguirinskaia, I., Lovejoy, S., Hubert, P., 2010. No monsters, no miracles: in nonlinear sciences hydrology is not an outlier!. Hydrol. Sci. J. 55, 965–979.
Sivakumar, B., 2004. Dominant processes concept in hydrology: moving forward. Hydrol. Process. 18 (12), 2349–2353.
Sivakumar, B., Jayawardena, A.W., Li, W.K., 2007. Hydrologic complexity and classification: a simple data reconstruction approach. Hydrol. Process. 21 (20), 2713–2728.
Sivakumar, B., Persson, M., Berndtsson, R., Uvo, C.B., 2002. Is correlation dimension a reliable indicator of low-dimensional chaos in short hydrological time series? Water Resour. Res. 38 (2).
Sivakumar, B., Singh, V.P., 2012. Hydrologic system complexity and nonlinear dynamic concepts for a catchment classification framework. Hydrol. Earth Syst. Sci. 16 (11), 4119.
Sivakumar, B., Singh, V.P., Berndtsson, R., Khan, S.K., 2015. Catchment classification framework in hydrology: challenges and directions. J. Hydrol. Eng. 20, A4014002.
Swain, J.B., Sahoo, M.M., Patra, K.C., 2016. Homogeneous region determination using linear and nonlinear techniques. Physical Geography, online.
Takens, F., 1981. Detecting strange attractors in turbulence. Lect. Notes Math. 898 (1), 366–381.
Tongal, H., Sivakumar, B., 2017. Cross-entropy clustering framework for catchment classification. J. Hydrol.
Trancoso, R., Phinn, S., McVicar, T.R., Larsen, J.R., McAlpine, C.A., 2018. Regional variation in streamflow drivers across a continental climatic gradient. Ecohydrology 10 (3).
Vignesh, R., Jothiprakash, V., Sivakumar, B., 2015. Streamflow variability and classification using false nearest neighbor method. J. Hydrol. 531, 706–715.
Vormoor, K., Lawrence, D., Schlichting, L., Wilson, D., Wong, W.K., 2016. Evidence for changes in the magnitude and frequency of observed rainfall vs. snowmelt driven floods in Norway. J. Hydrol. 538, 33–48.
Whitfield, P.H., 1998. Reporting scale and the information content of streamflow data. Northwest Sci. 72, 42–51.
Whitfield, P.H., 2012. Floods in future climates: a review. J. Flood Risk Manage. 5, 336–365.
Whitfield, P.H., et al., 2012. Hydrologic reference networks I. The status of national reference hydrologic networks for detecting trends and future directions. Hydrol. Sci. J. 57, 1562–1579.
Zbilut, J.P., Webber Jr, C.L., 1992. Embeddings and delays as derived from quantification of recurrence plots. Phys. Lett. A 171 (3–4), 199–203.